WIRELESS ENGINEER

Vol. 32 FEBRUARY 1955 No. 2

Radiation by Television and F.M. Sets

AN investigation into the many special forms of interference to which the superheterodyne is subject has recently been carried out by the British Radio Equipment Manufacturers' Association, with the aim of determining whether the use of a particular intermediate frequency for television receivers would be beneficial. As a result, it has recommended the general adoption in this country of 34·65 Mc/s for the vision intermediate frequency, with the local oscillator above the incoming signal; which automatically entails the use of 38·15 Mc/s for the sound intermediate frequency.

We do not propose to discuss in any detail the reasons for this choice; they have, in part, already been published[1]. We feel that they are very sound ones and that the final choice is a good one. We do, however, want to emphasize the importance of the universal adoption of these standard frequencies as soon as possible, for their potential benefit will not be realized until they are, in fact, the only ones in use anywhere.

Under the conditions of domestic reception, where receivers and aerials are in close proximity, it seems to be impracticable to prevent the local oscillator from radiating to a very appreciable degree. The only possible way of preventing it from causing interference is then so to allocate the frequencies of transmitters that in any area receiver oscillators will not be on frequencies which it is required to receive in that area.

It is not envisaged that more than two or three television stations will be receivable in any area in this country for a long time to come. This being so, if all receivers have the same intermediate frequencies, their oscillators will all be on certain particular frequencies and it will be possible in most, if not in all, cases to arrange that these frequencies of local radiation are allocated for transmissions in some remote area.

This possibility has been considered in the choice of intermediate frequency, but we do not feel that the importance of the universal employment of the same frequencies in all sets is sufficiently emphasized in the B.R.E.M.A. Report. It is, actually, the main reason for standardization.

It may be felt that, as the benefit from it depends upon a particular allocation of transmitting frequencies, it is an illusory one, for there are a good many other factors to be taken into account when assigning particular frequencies to stations. In any case, many frequencies are already allocated and in use and changes are difficult to effect.

It is, therefore, desirable to see how the standard intermediate frequencies fit into the existing pattern of frequencies. Table 1 shows the frequencies allocated for the vision carriers of Channels 1–13 and their present allocation, so far as it is known, together with the local-oscillator frequencies, and their second harmonics, for an i.f. of 34·65 Mc/s. The vision pass-band is approximately $+0{\cdot}5$ Mc/s to -3 Mc/s on these carrier frequencies and the sound carrier is at $-3{\cdot}5$ Mc/s. A band of $\pm 0{\cdot}25$ Mc/s is usually allowed for oscillator drift and this, of course, becomes $\pm 0{\cdot}5$ Mc/s for the second harmonic.

It is evident that there is no possibility at all of oscillator radiation from a receiver in Band I (Channels 1–5) causing interference with the reception of any other Band-I station, nor is there any possibility of fundamental-frequency radiation from a Band-I receiver interfering with Band-III (Channels 6–13) reception. The oscillator of a receiver of Channel 6, however, can interfere with reception of Channel 13 and it will be necessary to ensure that these two channels are not allocated to the same area.

It is necessary to consider more than television, however. Fundamental-frequency radiation from Band-I television receivers will fall in Band II

[1] "Television Intermediate Frequencies", *Wireless World*, December 1954, Vol. 60, p. 582.

and may interfere with f.m. sound broadcasting. Table 2 shows the frequency allocations for the proposed Band-II stations. The possibilities of interference would seem to be confined to radiation from receivers tuned to Channel 3; allowing for oscillator drift, radiation will be in the bands 91·15–91·65 Mc/s for the Kirk o' Shotts and Rowridge areas. This covers some of the Wrotham and Holme Moss Band-II frequencies. Holme Moss is probably too remote from both Kirk o' Shotts and Rowridge for there to be any trouble, but it looks very likely to occur on the Third programme from Wrotham in the Isle of Wight and South Coast area.

When second harmonics are considered, there are more possibilities of trouble. Table 1 shows that Channel-3 receivers may interfere with reception on Channel 7, 4 with 9 and 5 with 11. Third harmonics should cause no trouble. As well as avoiding allocating Channels 6 and 13 to the same area, therefore, Channels 7, 9 and 11 should not be allocated to areas served respectively by Channels 3, 4 and 5. As Table 1 shows, the present allocation for Channels 4 and 9 seems satisfactory; those for the other channels are, as yet, unknown.

TABLE 1

Channel	Vision Carrier (Mc/s)	Oscillator (Mc/s)	2nd Harmonic (Mc/s)	Allocated Area
1	45	79·65	159·3	London; N. Ireland
2	51·75	86·4	172·8	Holme Moss; Plymouth*
3	56·75	91·4	182·8	Kirk o' Shotts; Rowridge
4	61·75	96·4	192·8	Birmingham; Aberdeen
5	66·75	101·4	202·8	Wenvoe; Pontop Pike
6	179·75	214·4	428·8	
7	184·75	219·4	438·8	
8	189·75	224·4	448·8	Birmingham
9	194·75	229·4	458·8	London; Manchester
10	199·75	234·4	468·8	
11	204·75	239·4	478·8	
12	209·75	244·4	488·8	
13	214·75	249·4	498·8	

* *At present used by the Truleigh Hill Booster.*

TABLE 2

Programme			
Light (Mc/s)	Third (Mc/s)	Home (Mc/s)	Station
88·1	90·3	92·5	N. Hessary Tor (Devon)
88·3	90·5	92·7	Sutton Coldfield
88·5	90·7	92·9	Pontop Pike
88·7	90·9	93·1	Meldrum (Aberdeenshire)
88·7	90·9	93·1	Blaen Plwy (W. Wales)
89·1	91·3	93·5	Wrotham
89·3	91·5	93·7	Holme Moss
89·7	91·9	94·1	Norwich
89·9	92·1	94·3	Wenvoe*
90·1	92·3	94·5	Divis (N. Ireland)

* *Subject to confirmation.*

Radiation of harmonics by f.m. receivers for Band II may be much more serious. An intermediate frequency of 10·7 Mc/s seems a favourite one. If the oscillator frequency is above the signal, the television Channels 10, 11 and 12 are liable to suffer interference from the second harmonics of the oscillators of f.m. receivers tuned to no less than 21 of the 30 f.m. stations. There seems to be no possibility of avoiding such trouble by any minor change of intermediate frequency, nor by the allocation of transmitter frequencies to particular areas.

However, if the oscillator frequency is below the signal, the second-harmonic radiation will be in the band 154·8–167·6 Mc/s and the fundamental-frequency radiation in the band 77·4–83·8 Mc/s. It will, therefore, be just clear of Bands I and III.

If f.m. receivers with lowish intermediate frequencies are used to any extent, it seems to us imperative that the oscillators should be below the signal if three, at least, of the Band-III television channels are not to be unusable. The only alternative that we can see is for f.m. receivers to have an i.f. of the order of 20 Mc/s; both fundamental and second-harmonic oscillator radiation would then fall outside Band III.

One manufacturer of f.m. sets is actually using an i.f. of 19·5 Mc/s, but, so far as we know, only one.

We feel that B.R.E.M.A. has done a good job in standardizing 34·65 Mc/s for the vision i.f. of television receivers and that, when its use becomes general, it will largely eliminate oscillator radiation interference by television receivers in Bands I, II and III. We are wholeheartedly in favour of this standard. We do feel, however, that the job is only partly done until the problem of f.m. receiver radiation is tackled and that the time to do this is now, before large numbers of f.m. sets are in the hands of the public.

We have here considered radiation only as it affects television and f.m. receivers and ignored its possible effects on other services. This must, of course, be considered, but it is usually less serious, because the receivers concerned are generally more widely separated from the source of radiation.

The proper and only complete cure for the interference is to prevent broadcast receivers from radiating at all. Unfortunately, this appears to be too expensive a solution to be practicable.

W. T. C.

OBLIQUE-INCIDENCE PULSE TRANSMISSION

Over a 2,360-km Path via the Ionosphere

By J. W. Cox and Kenneth Davies

(Defence Research Telecommunications Establishment, Ottawa)

SUMMARY.—The pulsed multi-frequency ionospheric recording technique was used to obtain oblique incidence, delay time frequency records. Sweeps were taken at points 2,360 km apart during the period June to August 1949. Sweeps obtained during quiet and disturbed conditions are presented showing N type echoes, scatter propagation at frequencies about the m.u.f. and spread echoes. It was found that reciprocity held to a first approximation and that the strength of the Pedersen ray was often quite appreciable at frequencies well below the m.u.f. A test of the oblique-incidence transmission theory, as developed by Millington, has been made by converting vertical h'-f records to equivalent oblique records and comparing these with observation. There is good agreement between theory and observation. It is shown that the Sellmeyer dispersion formula is more accurate for the calculation of maximum usable frequencies than the Lorentz formula.

1. Introduction

MOST experimental work on the ionosphere, especially on the F region, has been carried out at essentially normal incidence with transmitter and receiver close together. Some of the most important early investigations were made at oblique incidence, but in most parts of the world it is easier to make observations at normal incidence. Oblique-incidence experiments have been made to check the theory of ionospheric transmission and it is now known that, in general, the accepted theories are qualitatively correct, though there is still much that is obscure.

Over much of Canada the ionosphere takes on a peculiar form. Regions of a type not seen farther south occur, and disturbances which are rare farther south are normal. Most of the measurements made by the accepted methods can be interpreted only with difficulty, and many not at all, in conventional terms. There are some qualitative reasons to suppose that oblique-incidence measurements would be easier to interpret; hence, it was decided to make such measurements. But, since this would involve working in relatively inaccessible areas, it was felt best to first make measurements in places more easily reached. While this would not necessarily contribute much to the solution of northern problems, it could be used to perfect techniques and, incidentally, to acquire further information on some of the doubtful points still unsettled in southerly observations.

Because of the limitations of available staff, it was possible to work only in the summer. Some preliminary measurements were made between Ottawa and London, Ontario, in the summer of 1948 and, on the basis of lessons then learnt, measurements were made between Ottawa and Saskatoon, Sask. in the summer of 1949. Unfavourable circumstances have prevented the continuation of the work as planned, and the measurements, which were originally considered preliminary are, therefore, being dealt with separately.

MS accepted by the Editor, August 1954

2. Methods

In planning the experiments, the following principles were considered:

(a) It is essential to measure the variations of all quantities with frequency. The arguments which historically replaced single-frequency by multi-frequency measurements at vertical incidence have even more force at oblique incidence.

(b) It is desirable to have some measurement of transmission time, as well as of transmission pattern. No sufficiently accurate time reference exists locally, so it must be built into the apparatus.

(c) Measurements should be made as rapidly as possible.

Of these, the third is probably at least as important as the others under the rapidly-changing conditions which prevail in the north, but since automatic multi-frequency apparatus was not available it was decided to accept the limitations of manual working. The methods adopted were essentially somewhat modernized versions of those developed by Eckersley in experiments which were terminated by the outbreak of war in 1939.

The principle is shown in Figs. 1 and 2. Each end had a transmitter and a receiver, continuously and independently variable over a frequency range 2 to 25 Mc/s (the upper limit was set by available equipment). Pulses were transmitted from each end at 25 pulses per second, the

repetition frequency was controlled by a crystal and the crystals were adjusted so that their frequencies were sufficiently close to ensure synchronization of pulses. This method was preferred to that of the responder technique, because it was unaffected by changes in echo pattern and amplitude. Since the apparatus was manually operated, there was always an operator present to correct small departures from synchronism.

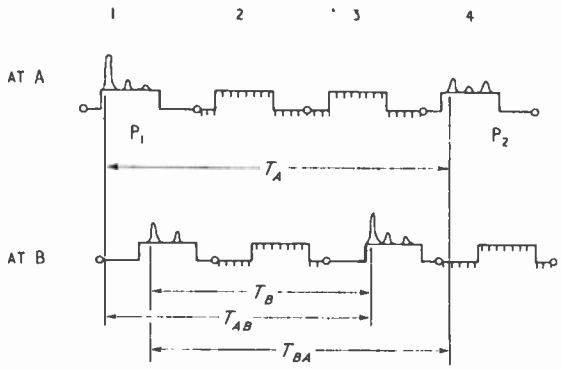

Fig. 1. *Timing cycle.*

At each end time-bases at 100 c/s were displayed on a cathode-ray tube, so that there were four traces in all between successive local pulses. On two of these the receiver output was displayed, and on the other two time-markers were placed. Pedestals were provided also with adjustable delay from the beginning of the time-bases, and arrangement was made, when required, to display only the top of the pedestal. Fig. 1 shows the arrangements at both ends, A and B, in the complete cycle of four sweeps. At A, the local pulse occurred on sweep 1, on pedestal P_1, and was displayed together with any vertical echoes. There were then two sweeps with time-markers; sweep 2 had a pedestal whose time delay from the beginning of the sweep was the same as P_1; sweep 3 had a different pedestal delay which was the same as the delay for the pedestal P_2 on sweep 4. Assuming that end B was transmitting in synchronism with A, its echoes would be received on P_2. Each of the four sweeps had an independent vertical shift on the face of the tube, and when the tops of the pedestal alone were shown, the appearance was as shown in Fig. 2.

This form of presentation was adopted to give sufficient resolution which was necessary for accurate measurement of the difference of path length between signals reflected by the ionosphere.

There are thus a number of pedestal and pulse delays to be measured, and these are shown in Fig. 1 where:—

T_{AB} is the time interval between the sending of a pulse from A and its reception at B.

T_{BA} is the time interval between the sending of a pulse from B and its reception at A.

T_A is the time interval between the sending of a pulse from A and the reception of a pulse from B.

T_B is the time interval between the sending of a pulse from B and the reception of a pulse from A.

From Fig. 1 it can be seen that:—

$$T_{AB} + T_{BA} = T_A + T_B \quad .. \quad .. \quad (1)$$

Since, to a first approximation, reciprocity holds (see Section 5)

$$T_{AB} = T_{BA} = T$$

Therefore,

$$T = \tfrac{1}{2}(T_A + T_B) \quad .. \quad .. \quad (2)$$

The transmitters used were conventional self-oscillators with about 10 kW peak output power contained in a 50-microsecond pulse. Communication receivers suitably modified for pulse reception were used and the indicators and timing circuits were derived by modifying and adding to standard Loran AN/APN4 equipment. The aerials at Ottawa were rhombics and at Saskatoon two horizontal dipoles were used. The latter were probably responsible for the apparent lack of response at very low angles.

The experiments were of two types. In the first type, both ends transmitted on the same frequency. Thus, each reading was complete in itself. It was found possible to maintain a schedule of one frequency per minute, and, in general, frequency steps 100 kc/s apart were used. In the second type, one end remained fixed on frequency while the other was altered. This made faster frequency shift possible, but could be used only if there was reason to believe that the delay on the fixed frequency would stay constant during the experiment.

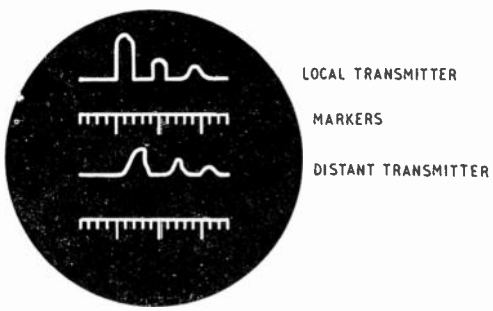

Fig. 2. *Oscilloscope display.*

3. Application of Vertical-Incidence Data to Oblique Transmission

The theory of transformation from vertical to oblique incidence has been dealt with by many authors, all of whose results are essentially

identical within the limitations of their assumptions. They normally deal either with an almost rigorous theory applied to a relation between ionization density and height (usually parabolic), or to a somewhat less rigorous method independent of the exact electron distribution. Both methods give practically the same results.

In order to deal with path-times at frequencies far removed from the m.u.f. it is easiest to use a theory not depending on the distribution near the maximum density, and consequently the transmission curve method of N. Smith[1] extended by Millington[2] was used. The appropriate transmission curve is shown in Fig. 3. The delay times shown are in excess of the delay time of the ground wave, if the latter could be observed.

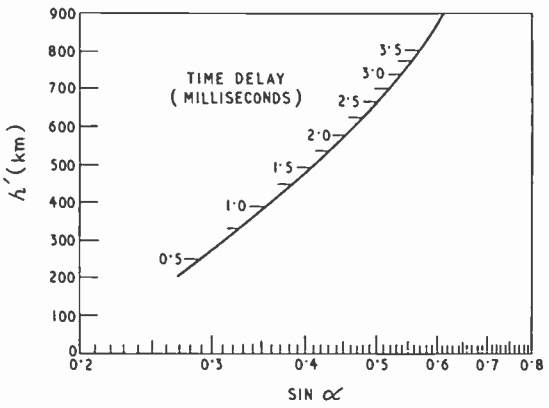

Fig. 3. *Transmission curve for distance of* 2,360 *km.*

4. Experimental Results

From the measurements described in Section 2 the transmission time, T, has been plotted as a function of frequency. Some typical plots are shown in Figs. 4 to 9.

Fig. 4 shows a classically expected case, with clear echoes, 'magneto-ionically' split, and reflected from one layer only.

Fig. 5 is typical of a quiet day, with both F_1 and F_2 present, but the skip frequency for F_2 is greater than for F_1.

Fig. 6 shows a slightly disturbed day on which the F_2 density was reduced, whereas the F_1 density was not reduced much. The skip frequency for the distance depended on F_1.

Fig. 7 shows the occurrence of an N echo; i.e., an echo with one reflection from E and one from the ground. This is identified by its delay, and an extension of the theory mentioned in Section 3. It may be remarked that M echoes (one intermediate E reflection not touching the ground) may have occurred in other sweeps but at this distance they are difficult to distinguish from second-order F echoes.

Figs. 8 and 9 show progressively increasing 'spread echoes'. In Fig. 8 there is a clear 'classical' penetration, but the actual m.u.f. is nearly 2 Mc/s higher. In Fig. 9 the spread completely obscured the classical penetration. The Pedersen ray is present (delay 1·8 milliseconds at 15 Mc/s) in this example, though often completely obscured.

Fig. 9 is a good example of the need for multi-frequency records. It would scarcely be possible to identify the echoes at, say, 16·2 Mc/s on the basis of records at that frequency only.

Before trying to relate our results quantitatively with those obtained at vertical incidence, the following important points should be noted:

(a) The Pedersen ray is of importance. It is of strength comparable to that of the main ray over a large range of frequency, and is often seen more than 25% in frequency below the m.u.f.

(b) The magneto-ionic separation between ordinary and extraordinary m.u.fs is less at oblique than at vertical incidence. In the best ten records showing unambiguous penetration, the separation between m.u.fs averaged 0·29 Mc/s in about 15 Mc/s.

(c) 'Spread echoes' are obtained at considerable obliquity and must be allowed for in calculating m.u.fs.

(d) E echoes were not observed, although the season was favourable, especially for E_s, and the distance not geometrically too great. Too much emphasis should not be placed on this fact as the aerials used were not favourable to low-angle radiation.

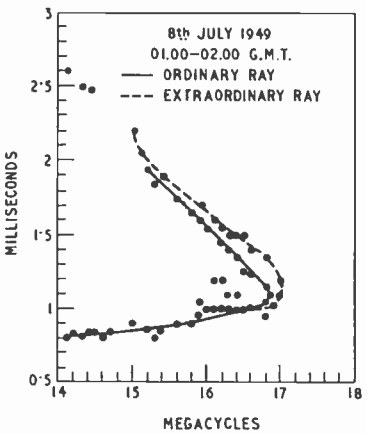

Fig. 4. *Classical form of oblique-incidence record.*

5. Reciprocity

The points made in the foregoing section refer to transmission in one direction only just as well as to the double transmission in both directions. It is inherent in the theory that a certain type of

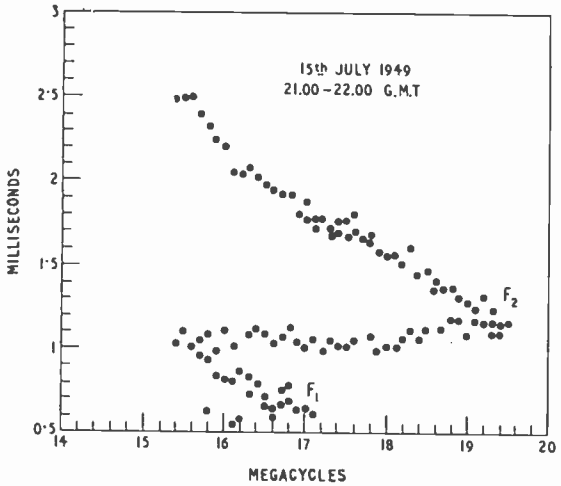

Fig. 5. *Record of typical quiet day.*

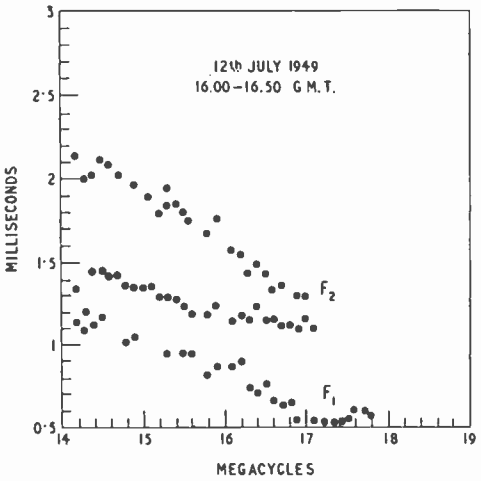

Fig. 6. *Record with reduced F_2 density.*

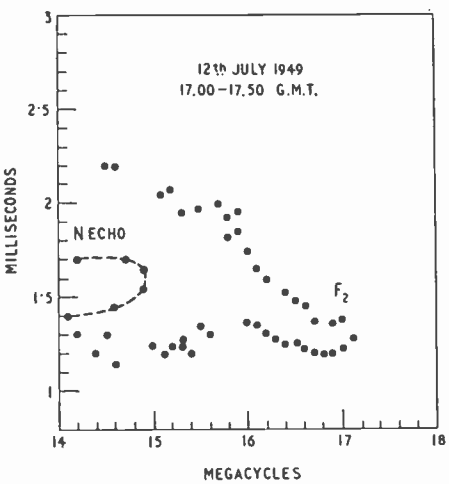

Fig. 7. *Echo with one E and one ground reflection.*

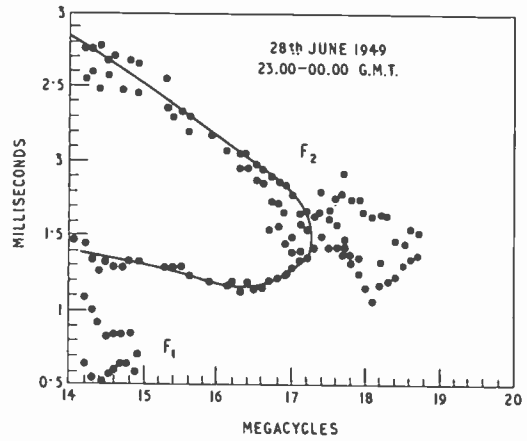

Fig. 8. *Spread echo giving a m.u.f. 2 Mc/s above normal.*

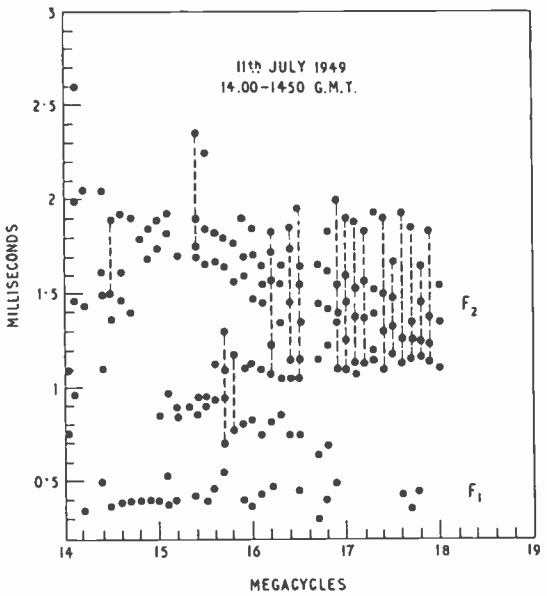

Fig. 9. *Spread echoes which obliterate the classical penetration.*

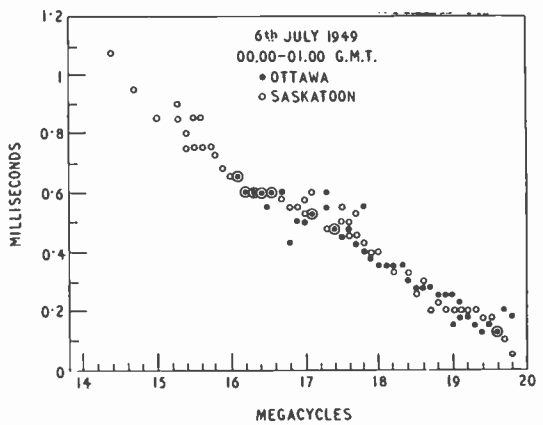

Fig. 10. *Delay between low-angle and Pedersen rays;* ●*measured at Ottawa,* ○*measured at Saskatoon.*

reciprocity should prevail. One does not expect to obtain equal amplitudes or polarizations at the two ends and, in fact, it was often noticed that a particular echo was only seen at one end. Without detailed measurements of aerial polar diagrams and of noise, no deductions can be made from this. It would be expected that the path-times in each direction would be identical. This cannot be exactly measured, since there is no common reference of timing. A previous check (Eckersley et al.[3]) measured only the m.u.f. It is assumed that the Pedersen ray, which is greatly delayed in the ionosphere, would be liable to be affected by any non-reciprocity much more than the low-angle ray, and therefore simultaneous measurements of the separation between the two rays have been made as a function of frequency on a number of occasions. A typical result is shown in Fig. 10. It is seen in this figure that the delays in the two directions are identical within the limits of measurement, even though the transmission was stronger (extends to lower frequencies) in one direction than the other.

Although it is probable that this particular path-separation would be more sensitive to non-reciprocity than most others. Similar checks can be made at any time when more than one echo is present. Checks were, therefore, made on all possible occasions when the echoes were clean and not spread. No measurable departure from reciprocity was ever observed.

6. Relation of Oblique Records to Vertical-Incidence Records

By means of the transmission theory mentioned in Section 3 and the transmission curve of Fig. 3 it is possible to transform between vertical and oblique incidence. To check the validity of the theory transformation in only one direction is necessary, but some examples are given of both types of transformation as each shows the magnitude of certain appropriate features. Figs. 11(a) and 11(b) are the observed oblique records, together with the curves deduced from vertical-incidence recordings made, not at the mid-point as would be desirable, but at Ottawa with an allowance of one hour for the time difference between the local time at the mid-point and the local time at Ottawa.

The agreements between the deduced and observed values in Figs. 11(a) and (b) are very striking, particularly insofar as the maximum frequencies are concerned. The deduced and observed time delays are also in very good agreement especially when it is realized that the F_2 layer varies considerably with longitude and latitude.

On these sweeps the agreement is nearly as good as the accuracy of the measurements, especially for the time-delay of low-angle rays.

In Fig. 12 are shown some of the results of the oblique to vertical transformation, similarly compared. Here again it will be seen that the agreement is of the order of magnitude of the fairly rapid fluctuations of the ionosphere, and therefore good enough for practical purposes.

7. Lorentz and Sellmeyer Polarizations

There has been considerable discussion in the literature as to whether the 'Lorentz term' should be included in ionosphere theory. Newbern Smith[4], including the magnetic field in a special case, and Beynon[5], excluding the magnetic field, have shown that a considerable difference between the two theories is to be expected at sufficiently oblique incidence.

Both authors adduce experimental evidence that the Lorentz term is small, but both have to admit uncertainty as to the actual vertical-incidence data for the regions they studied. In Beynon's case this was the F_2 region, not sounded at the mid-point, and in Smith's case it was assumed to be the E layer near sunrise when complications are often present in E.

The agreement between our oblique and vertical

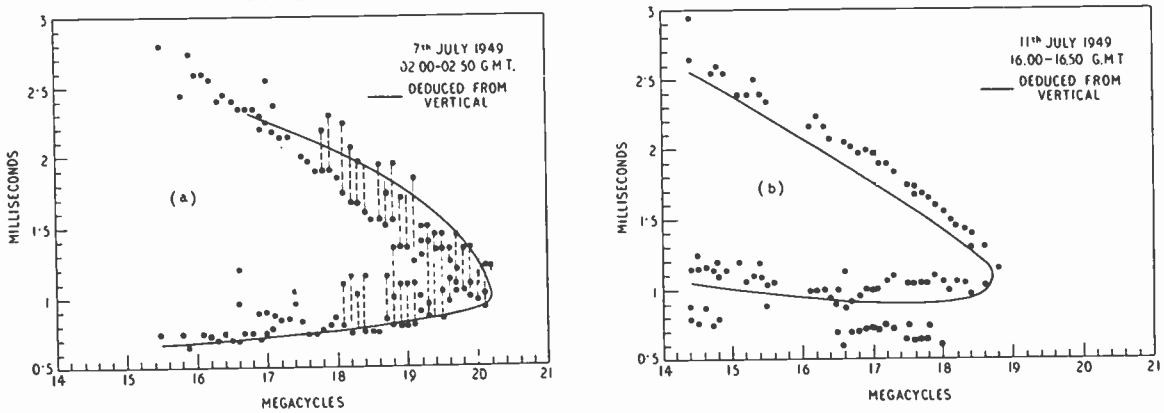

Fig. 11. *Comparison between observed and deduced oblique curves.*

results shown in Section 6 could be taken as sufficient proof that the Lorentz term should be zero or at least very small. However, the agreement is not perfect, and our results in Section 6 are subject to the same criticism as those of the other authors. However, using Beynon's calculations for a parabolic region of semi-thickness 100 km and a height of maximum

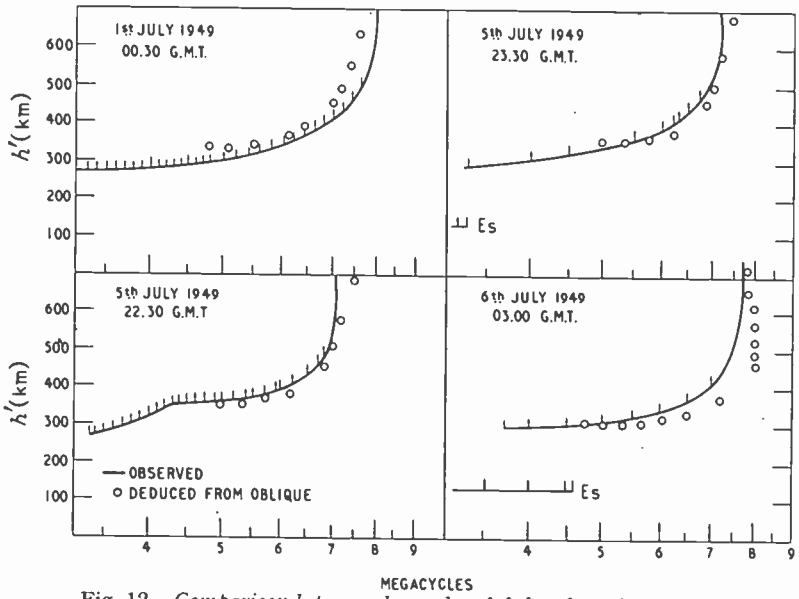

Fig. 12. *Comparison between observed and deduced vertical curves.*

electron density of 350 km the following values for the skip frequency factor for a number of results have been obtained:—

F_2

Source	Value
Sellmeyer theory	2·80
Lorentz theory	3·50
Experimental (for Ottawa)	2·69
,, (for Saskatoon)	2·56

This is in favour of the Sellmeyer theory. However, the measurements of F_2 are such that it is still somewhat uncertain.

Fortunately it is possible to identify unambiguously the F_1 region penetration. This is excellently adopted for checking on the theory. Since the F_1 region is regular in behaviour an estimate on the mid-point value of f_0F_1 should be very accurate.

Again using Beynon's results with semi-thickness 50 km and a height of maximum of 250 km the following values of the m.u.f. factor were obtained:—

F_1

Sellmeyer theory	3·51
Lorentz theory	4·27

Using these factors, the mean diurnal variation of f_0F_1 during the period of the work were deduced from the observed penetration frequencies of F_1 and the values thus obtained are compared with the observed means from Prince Rupert, British Columbia, and St. John's, Newfoundland, which straddle the mid-point in latitude, and were reliable stations for that month.

The comparison is shown in Fig. 13, from which it appears that the agreement with the Sellmeyer theory is very close, and rules out the Lorentz theory.

Conclusions

The conclusions deduced from this work are:—

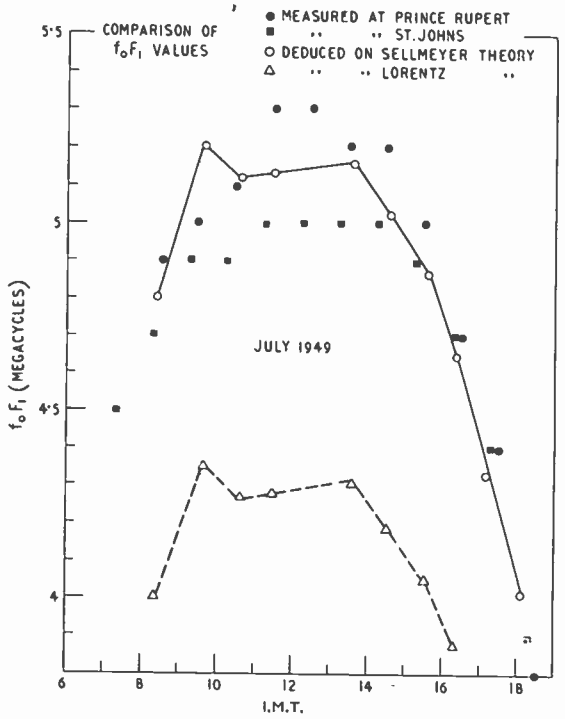

Fig. 13. *Comparison between Lorentz and Sellmeyer theories.*

(1) The theory of transmission at present in use is sufficiently accurate for practical purposes when the ionosphere is quiet.
(2) Reciprocity is valid.
(3) Sellmeyer theory is applicable.
(4) The Pedersen ray is relatively strong at frequencies well below the penetration frequency.
(5) Spread echoes are common at oblique incidence, and occur at frequencies above the normal penetration frequency.
(6) The magneto-ionic separation at this distance is about 0·29 Mc/s.

Acknowledgments

This work was performed under Defence Research Board Project No. D48-95-11-02; we are indebted to the Defence Research Board of Canada for permission to publish this paper, and to the University of Saskatchewan for providing us with the site and other facilities at Saskatoon.

REFERENCES

[1] N. Smith, *Proc. Inst. Radio Engrs*, 1939, Vol. 27, p. 332.
[2] G. Millington, *Proc. Phys. Soc.*, 1938, Vol. 50, p. 810.
[3] T. L. Eckersley, S. Fallon, F. T. Farmer, W. O. Agar, *Nature*, 1940, Vol. 145, p. 222.
[4] N. Smith, *Bur. Stand. J. Res. Wash.*, 1941, Vol. 26, p. 105.
[5] W. J. G. Beynon, *Proc. Phys. Soc.*, 1947, Vol. 59, p. 97.

FERROMAGNETIC LOOP AERIALS

For Kilometric Waves

By J. S. Belrose

SUMMARY.—The design of ferromagnetic loop aerials for the frequency range 80–200 kc/s is approached with a view to maximizing their signal-to-noise ratios. These considerations are related to experimental results on loop aerials using ferromagnetic cores of various types. Sensitivities of 1 μV/m (for receiver bandwidths of 100 c/s) for a 10-db signal-to-noise ratio are shown to be possible.

Introduction

THE physical size of a loop aerial may be greatly reduced by employing a ferromagnetic core to concentrate the magnetic flux. An excellent engineering approach to the analysis of the performance of these magnetic rod aerials for reception of medium waves has been given by van Suchtelen[1]. No precise information is available concerning the use of such aerials at low frequencies. The purpose of this paper is to outline the design considerations for ferromagnetic loop aerials for reception of low-frequency waves in the range 80–200 kc/s, and to relate these considerations to some experimental results on loop aerials using ferromagnetic cores of various types.

The most important single factor in radio reception is the signal-to-noise ratio at the output terminals of the receiving amplifier. It is imperative that the absolute sensitivity of the receiving system be limited by atmospheric noise and not by the thermal fluctuation noise originating in the resistive elements of the aerial and associated coupling circuits. Since the effective height of a small ferromagnetic loop aerial is very small at low frequencies it is necessary to analyse the loop-aerial circuit with a view to maximizing the signal-to-noise ratio, where the noise is the thermal fluctuation noise introduced in the loop-aerial circuits. Since practical and economic considerations lead to the use of a rod or tube of small physical dimensions, this type of ferromagnetic core is considered. The experiments were made using Ferroxcube rods and tubes of various dimensions, supplied by Philips' Industries, Eindhoven. The various magnetic parameters of Ferroxcube material which affects the performance of the loop aerials, such as permeability factors, loss tangents, and temperature coefficients, are drawn from van Suchtelen's papers[1,2].

MS accepted by the Editor, March 1954

Basic Formula

The voltage e_s between the terminals of a small loop aerial, consisting of several turns, due to a changing magnetic field is related to the magnetic flux through a surface enclosed by the loop by

$$e_s = -N\frac{d\Phi}{dt} \qquad \ldots \quad \ldots \quad \ldots \quad (1)$$

where N = number of turns
Φ = magnetic flux enclosed by the loop, webers*
e_s = e.m.f. induced in the loop aerial, volts (subscript s used here to designate signal voltage as opposed to noise voltage e_n to be introduced later).

For sinusoidal time varying fields

$$e_s = -j\omega\Phi N$$

where $\omega = 2\pi f$
f = wave frequency, c/s.

*The rationalized m.k.s. system of units is used.

The time factor $e^{j\omega t}$ has been dropped. It is clear that e_s and Φ can be either maximum or r.m.s. values. All values used here will be r.m.s. since in communication engineering the r.m.s. value of voltage is generally used (certainly when concerned with thermal noise).

Now the flux threading the loop

$$\Phi = BA$$

where B = magnetic flux density in free space, webers/m^2

A = area in m^2

Hence

$$e_s = \omega BAN \quad .. \quad .. \quad .. \quad (2)$$

where the factor $-j$ has been omitted.

By introducing a ferromagnetic core the flux density B threading the loop aerial can be increased. Analysis shows that this core should be more or less in the form of a rod[4,5,6], as indicated in Fig. 1, to achieve a satisfactory increase in B, and concentrate the lines of force through the turns of the coil.

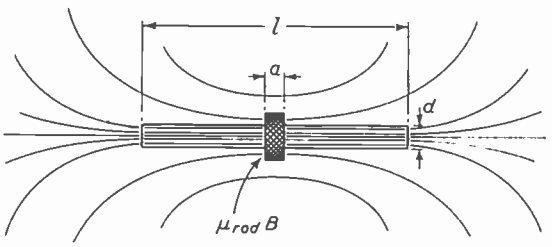

Fig. 1. *Ferromagnetic loop wound on a rod. The aerial consists of a core of length l and diameter d on which is wound a coil of length a.*

If the flux density is increased by a factor μ_{rod}, the apparent permeability of a rod-shaped core, then the voltage induced in the loop will be

$$e_s = \omega BAN\,\mu_{rod} \quad .. \quad .. \quad .. \quad (3)$$

For a travelling plane electromagnetic wave in free space

$$\frac{E_s}{H_s} = \sqrt{\frac{\mu}{\epsilon}} = 120\pi \quad .. \quad .. \quad .. \quad (4)$$

where μ = permeability of free space = $4\pi \times 10^{-7}$ henrys/m

ϵ = dielectric constant of free space = $1/36\pi \times 10^{9}$ farads/m

E_s = electric field intensity, volts/m

H_s = magnetic field intensity, amperes/m.

Also

$$B = \mu H_s \quad .. \quad .. \quad .. \quad (5)$$

Substituting Equs. (4) and (5) in (3)

$$e_s = \frac{2\pi AN}{\lambda}\mu_{rod}E_s \quad .. \quad .. \quad .. \quad (6)$$

where λ = wavelength, metres = c/f

c = velocity of light, m/s.

This can be written

$$e_s = h_e\mu_{rod}\,E_s = h_{eff}\,E_s \quad .. \quad .. \quad (7)$$

where h_e = effective height of loop aerial without the ferromagnetic core

h_{eff} = apparent effective height of ferromagnetic loop aerial.

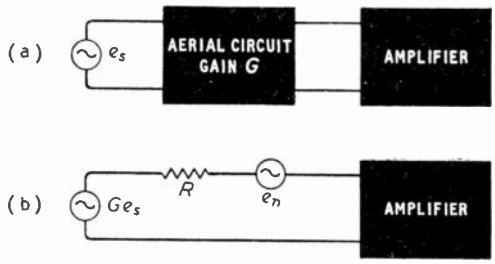

Fig. 2. *General aerial coupling circuit.*

The loop aerial is now coupled to a good amplifier* through a coupling circuit of gain G, as shown in Fig. 2(a). This arrangement may be represented by the equivalent circuit of Fig. 2(b); where R is the resistive component of the input impedance and e_n is the thermal noise voltage produced in the noise-free resistor R. The thermal noise voltage is given by

$$e_n = (4KTR\Delta f)^{\frac{1}{2}}$$

where K = Boltzmann's constant = $1{\cdot}37 \times 10^{-23}$ watt-sec/degree

T = absolute temperature, degrees Kelvin

R = resistive components of input impedence, ohms

Δf = effective bandwidth as seen by detector, c/s.

For a system at room temperature (17°C)

$$e_n = 1{\cdot}26 \times 10^{-10}\sqrt{R\Delta f} \quad .. \quad .. \quad (8)$$

The signal-to-noise ratio at the input terminals of the amplifier is then

$$\gamma = \frac{Ge_s}{e_n} = \frac{Ge_s}{1{\cdot}26 \times 10^{-10}\sqrt{R\Delta f}} \quad .. \quad (9)$$

For the case of a directly-tuned loop, which consists of an inductance L_0 resonated to the operating frequency f_0 by a capacitance C_0 the gain G, when the output is measured across C_0, is Q_0. The resistance R, of Equ. (9) is

$$R = Q_0\omega_0 L_0 \quad .. \quad .. \quad .. \quad (10)$$

Substituting Equs. (6) and (10) in Equ. (9) we obtain

$$\gamma = \frac{66{\cdot}3\,NA\mu_{rod}}{\sqrt{\Delta f}}\sqrt{\frac{Q_0 f_0}{L_0}}\,E_s \quad .. \quad (11)$$

The inductance of a coil with a ferromagnetic core is

$$L_0 = kN^2\,d\,\mu_{coil} \quad .. \quad .. \quad .. \quad (12)$$

where d = diameter of coil

k = constant which depends on the form factor of the coil[3]

*At low frequencies if the first stage of the receiver (i.e., aerial stage) has sufficient gain the signal-to-noise ratio of the entire system is that of the first stage.

μ_{coil} = coil permeability factor.

Substituting Equ. (12) in Equ. (11)

$$\gamma = \frac{52{\cdot}1\,\mu_{rod}}{\sqrt{\Delta f}} \sqrt{\frac{Q_0 f_0 d^3}{k\,\mu_{coil}}}\, E_s \qquad .. \quad (13)$$

Analysis of this equation is difficult due to the interdependence of the various parameters. However, for a given application several of the parameters can be approximately fixed by other circuit requirements. The optimum Q-factor for the aerial circuit depends to some extent on the impulse performance of the amplifier. The bandwidth of the first stages of the amplifier should not be too narrow, otherwise trouble will be encountered by ringing of the circuits during signal reception in the presence of atmospheric noise of an impulsive nature. The impulse noise should be limited before the bandwidth is narrowed. In general, experience shows a bandwidth of 1–1·5 kc/s is about optimum for the loop circuit. The detector bandwidth Δf is fixed by the information-capacity requirements of the circuit. Therefore fixing these parameters the signal-to-noise ratio

$$\gamma = \text{constant} \times \mu_{rod} \sqrt{\frac{d^3}{k\,\mu_{coil}}} \qquad .. \quad (14)$$

It will be seen later that a rod having a large length to diameter ratio of a material of high initial permeability* should be used. Also the diameter should be as large as is practical, and finally the quantity $k\,\mu_{coil}$ should be as small as possible. As some of these factors are interrelated a compromise is necessary to obtain the maximum signal-to-noise ratio. For example, a reduction in the factor k by increasing the spacing between turns leads to a higher value of μ_{coil} and a lower value of μ_{rod}. It is shown later that optimum signal-to-noise ratio is obtained with a short coil near the centre of the rod.

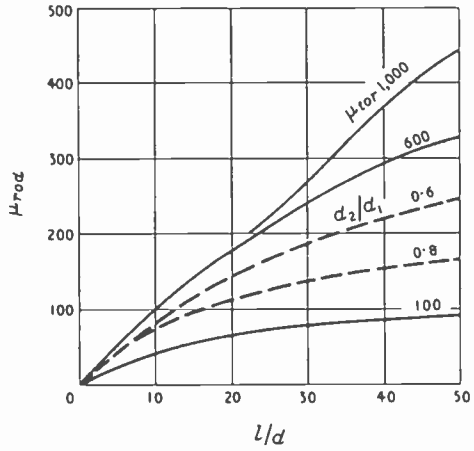

Fig. 3. *Rod permeability μ_{rod} as a function of the ratio l/d with the initial permeability μ_{tor} as a parameter. The solid curves are for rods. The dashed curves are for tubes where $\mu_{tor} = 600$ and the ratio d_2/d_1 refers to inside/outside diameter ratio of the tube.*

*Core materials having a very high initial permeability (1,000) can be used at low frequencies. The acceptable loss tangent usually limits the core permeability values to about 200 for medium-wave reception[1].

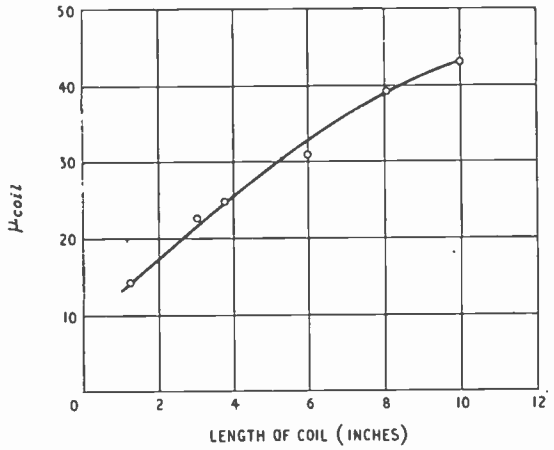

Fig. 4. *Graph showing the relation between coil permeability μ_{coil} and the length of the coil a. This is experimental for a specific rod 12 in. long (see text).*

Electromagnetic Properties of Ferroxcube

Rod Permeability

The initial permeability of the material, as stated by the manufacturer, gives the magnetizing force to flux density relationship as measured on a closed magnetic circuit; i.e., μ_{tor} which is the toroid permeability. The rod permeability μ_{rod} is a function of the toroid permeability of the material used and the physical dimensions of the rod. The theoretical expression relating these parameters is readily calculated if the rod is approximated by a solid spheroid (see Wait [4,5]). It is only necessary to assume that the spheroid is equivalent to the rod if the coil radii and the volume are the same. The graph shown in Fig. 3 has been calculated from graphs given by Wait [4,5] and van Suchtelen[1]. The relationship is shown (solid curves) between the rod permeability and the length/diameter ratio with the initial permeability as a parameter. The two dashed curves are drawn for tubes (for the case where $\mu_{tor} = 600$). The ratio d_2/d_1 is the inside/outside diameter ratio of the tube. It is clear that for both rods and tubes a large l/d-ratio should be used in order to realize a high value for μ_{rod}.

The distribution of flux density over the length of the rod will be almost parabolic for long rods, being maximum at the centre of the rod, and decreasing toward the ends. Hence if the value for μ_{rod} from Fig. 3 is used with Equ. (13) the length of the coil must be quite short and placed at the centre of the rod where the flux density is $\mu_{rod}B$. If the turns are spread out over

the rod the effective value of μ_{rod} will be reduced (by a factor 0·707 if $a/l = 1$).

Coil Permeability

The coil permeability μ_{coil} will depend on the rod permeability of the material, the ratio a/l of the length of the coil to the length of the rod, and on the position of the coil on the rod. For a short coil μ_{coil} will be small with respect to μ_{rod}. For a very long coil μ_{coil} will approach the value of μ_{rod}. The measured variation of μ_{coil} with the coil length a, for a particular sample core, is shown in Fig. 4. The rod was of Ferroxcube type IIIB2 material having an initial permeability of 600, a diameter of 1 in., and a length of 12 in. Using these values in conjunction with Fig. 3 it will be seen that the value of μ_{rod} is about 120.

Temperature Coefficient

Ferromagnetic materials of high permeability are not stable with temperature. If large changes of temperature are expected care should be taken to keep the factor μ_{coil} low. An expression relating the temperature factor of Ferroxcube with a small air gap is given by van Suchtelen[1]. If our loop aerial has an operating bandwidth of 1 kc/s and the maximum drift to be allowed is say ± 50 c/s at 200 kc/s for a temperature change of 30°C, then it can be shown that for Ferroxcube type IIIB2 (or IIIB3) material μ_{coil} should not exceed 12. For rods the temperature coefficient will be higher than the toroidal value. However, it is clear that μ_{coil} must not be too high (say about 25).

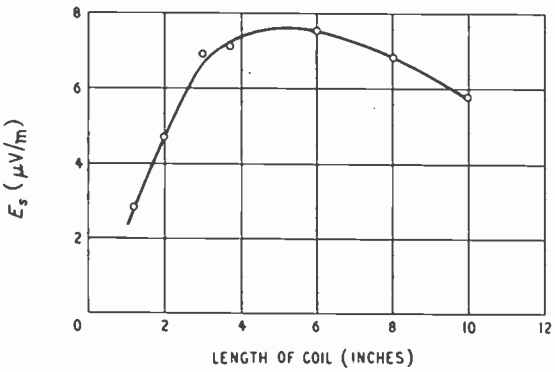

Fig. 5. *Graph relating the sensitivity of the aerial to the coil length. This is for a specific rod (see text).*

Experimental

General

In practical measurements the sensitivity of the aerial is estimated by calculating the external signal field intensity E_s necessary to give a signal-to-noise ratio of 10 db. That is the external field intensity necessary to produce in the output bandwidth of the amplifier a signal-to-noise ratio of 10 db. If this external field intensity is lower than the lowest expected atmospheric noise field intensity at the receiving location (i.e., the absolute sensitivity of the receiving system is determined by atmospheric noise) the aerial can be considered adequate for use in a communication point-to-point circuit.

The signal-to-noise ratio of the ferromagnetic loops considered here were measured as follows. The loop and measuring equipment were placed in a screened room. A known induction field was set up using a small test loop and a standard signal generator, General Radio type 1001-A. Two 5-ft lengths of coaxial cable were used to connect the loop to the amplifier. The centre-tap of the loop was earthed and the circuit tuned to the measurement frequency, 150 kc/s, by means of a small capacitor. One side of the loop was connected to the grid of the amplifier valve, thus utilizing only one half the available voltage across the capacitor, but maintaining balance to earth. The anode circuit of the amplifier was also tuned to the measuring frequency by a double-tuned critically-coupled transformer. This in turn was coupled to a cathode follower and the signal and noise output voltages were measured using a Stoddart type NM-10A noise/field intensity meter (used here as a microvoltmeter). The effective bandwidth of the recording system was about 400 c/s. The time constants of the indicating meter circuits are such that the meter shows a voltage which is the average of the input signal over 600 milliseconds continuously. The signal field intensity E_s required to produce a 10-db signal-to-noise ratio was recorded for each aerial.

Optimum Length of Coil

A Ferroxcube rod of type IIIB2 material approximately 12 in. long and 1 in. diameter was used for the experiments. Each of the test coils was wound with 10/38 litz wire, the coil diameter being approximately the same as the rod. A frequency of 150 kc/s was used. The results are presented in Table 1. Since the actual results were not directly comparable, because the inductance values are not quite constant, the results were corrected using Equs. (11) and (12) so that all values shown for E_s correspond to an inductance of 3·35 mH. The quantity $k\,\mu_{coil}$ is assumed unchanged for each correction.

The results are plotted in Fig. 5 where E_s is plotted as a function of the length a of the coil. It is readily seen that it is desirable to use a short coil. It is seen from Table 1 that the Q-factor falls off as the length of the coil is increased, however, if we assume that the Q-factor could have been maintained the general trend of the curve is not changed.

TABLE 1

Experimental Determination of Optimum Coil Length

Coil Length (inches)	No. of turns	Q_0	L_0 (mH)	μ_{coil}	E_s (μV/m)
1·125	125	100	3·47	14·4	2·8
2	113	100	3·4	16·8	4·7
3	120	83	3·59	22·4	6·8
3·875	120	71	3·66	24·4	6·8
6	132	58	3·35	30·4	7·6
8	128	71	2·92	39·2	4·7
10	120	71	1·6	43·1	5·8

Optimum Location on the Rod for Short Coil

As previously mentioned the factor μ_{coil} depends on the position of the coil on the rod. Since μ_{coil} is reduced as the displacement x from the centre of the rod is increased, it might be considered that an improvement could be obtained by shifting the coil from the centre of the rod. In Fig. 6 is shown the dependence of μ_{coil} and Q_0 on the displacement x. Here Q_0 and μ_{coil} are plotted as a function of $2x/l$. It is seen that both μ_{coil} and Q_0 are going in the right direction to achieve an improvement; i.e., μ_{coil} is decreasing and Q_0 is increasing. However, the sensitivity remains essentially constant as is shown by the curve for E_s. This implies that the reduction in the flux density $\mu_{rod}B$ threading the turns of the coil by displacing the coil from the centre effectively cancels the expected improvement. (Note that the values of E_s shown in Fig. 6 are higher than elsewhere in the paper for the case of a short coil on a 12-in. rod. The measurements here were made with a Stoddart field intensity meter NM-20A whose bandwidth is about 2 kc/s and hence the recording bandwidth is not independent of the loop-aerial bandwidth but the effective bandwidth of the system depends on that for the loop aerial, its amplifier, and the recording meter. These effects, however, would tend to show a better sensitivity at large values of $2x/l$ because of the increased Q-factor for the loop aerial, and so further support the above deductions.)

Examination of Rods and Tubes

Experiments of the type described above were made with the following materials:

(1) Rod. Length 12 in.; diameter 1 in.; material Ferroxcube type IIIB2; μ_{tor} 600; temperature factor 3×10^{-6}.

(2) Rod. Length 12 in.; diameter 1 in.; material Ferroxcube type IIIB3; μ_{tor} 600; temperature factor 3×10^{-6}.

(3) Tube. Length 12 in.; o.d. 1·42 in.; i.d. 1·1 in.; material Ferroxcube type IIIB2.

(4) As in (3) only of length 18 in.

(5) Tube. Length 12 in.; o.d. 1·77 in.; i.d. 1·456 in.; material Ferroxcube IIIB4; μ_{tor} 600; temperature factor 4×10^{-6}.

(6) Same as (5) only of length 18 in.

The results are shown in Table 2. The column E_s (normalized) is the sensitivity related to a common Q-factor of 100 for a fair comparison. The last column shows the signal field intensity required to produce a 10-db signal-to-noise ratio in a received bandwidth of 100 c/s. This has been calculated from the experimental results by the usual square root of the bandwidth relation which is applicable for signals in thermal noise.

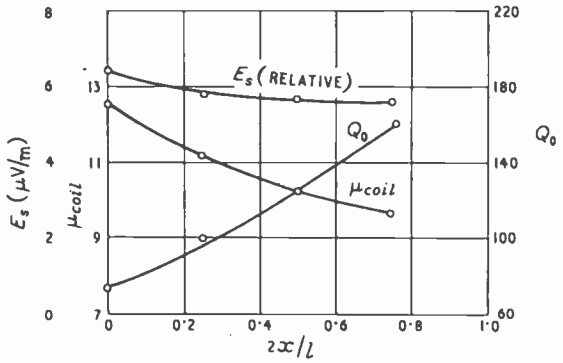

Fig. 6. *Graph showing the variation of important circuit parameters with the position of the coil on the rod. The coil length is 1¼ in.*

It is seen that a better sensitivity is obtained with the tubes. This is due to the increased

TABLE 2

Experimental Results for Rod and Tube Aerials

Type No.	Q_0	E_s (measured) (μV/m)	h_{eff} (m)	μ_{coil}	E_s (normalized) $\Delta f = 400$ c/s (μV/m)	E_s $\Delta f = 100$ c/s (μV/m)
1	77	4·6	0·009	12	4	2
2	100	4·1	0·0086	12·3	4·1	2·05
3	158	1·6	0·041	10·5	2	1
4	143	1·9	0·057	8·5	2·3	1·15
5	125	1·4	0·13	11·8	1·6	1·3
6	110	1·3	0·128	8·8	1·3	0·65

cross-sectional area of the coil. However, the effective permeability μ_{rod} is reduced for tubes due to the reduction of l/d, and due to the reduction of the cross-sectional area of the material. Examination, however, shows that the effective flux threading the coil must be little reduced by hollowing out the core. This is clear on inspection of the curves for tubes as shown in Fig. 3. Since the l/d-ratios are quite small and the toroidal permeability high there is only a small reduction in μ_{rod} when using a hollow core rather than a solid core. We note that for the 12-in. tubes the smaller diameter gives the better performance, whereas with the 18-in. tubes the larger diameter tube is better. This is due to the dependence of μ_{rod} on the l/d ratio.

Comparison with Theoretical Results

In a recent paper Wait[5] considers the problem of a receiving loop wound on a hollow prolate spheroidal core. This will approximate a hollow cylindrical rod-type core provided the l/d-ratio is not too small. Since the hollow prolate spheroid with the same volume and coil radius as the tube is a convenient model, values of the factor μ_{rod} can be calculated. Two such curves for tubes having an inside/outside diameter ratio of 0·6 and 0·8 (see Fig. 3) have been plotted. A relative measure of the pick-up voltage e_s for a given field intensity may then be calculated from Equ. (3)

$$e_s = \text{constant} \times A\,\mu_{rod}$$

where A = area of coil.

The value of this quantity has been calculated for the materials used in the experiments above and the results are given in Table 3, together with the relative values of $1/E_s$ obtained by experiment. To a first approximation these results should be directly compared as the quantity $1/E_s$ also gives a measure of the pick-up voltage. The theoretical and experimental results show the same general trend. There are individual discrepancies, but this is to be expected since the noise signal is not quite constant for each case.

TABLE 3

Theoretical Justification of Results

Type No.	E_s (relative) (μV/m)	Theoretical Calculations		Experimental
		μ_{rod}	$A \times \mu_{rod}$ (relative values)	$1/E_s$ (relative values)
1	4	120	25	25
2	4·1	120	25	24
3	2	60	26	50
4	2·3	100	37	43
5	1·6	48	31	62
6	1·3	76	50	77

Polar Diagram

The measured horizontal polar diagram of the loop is little different from the usual figure-8 pattern characteristic of loop aerials, even with the unconventional shape of the aerial. This means that capacitive pick-up is quite small. No experiments were done on electrostatically screening the aerial. For outside use an aluminum screen arranged so that no closed circuit encloses the turns of the loop aerial, for example, a slotted tube, would be desirable both to weatherproof the aerial and reduce precipitation-static effects.

Conclusions

Loop aerials of small physical size and moderate sensitivity can be obtained at low frequencies (80–200 kc/s) by using ferromagnetic cores of high permeability. The optimum form for these aerials is a short coil at the centre of a long thin rod or tube. For signal reception in a 100-c/s bandwidth (adequate for manual morse radio telegraphy or narrow-band frequency-shift keyed systems) an external field intensity of 1 microvolt per meter will produce a 10-db rise of signal above the background thermal noise of the amplifier (for an aerial wound on a 12-in. tube, see Table 2).

Acknowledgments

This work was carried out while the author was employed with the Defence Research Telecommunications Establishment, at the Radio Physics Laboratory, Ottawa, Canada. This paper is published with their permission. The author wishes to express thanks to Dr. J. R. Wait for the calculations presented in Table 3, and to Mr. J. McNally who made most of the experimental measurements.

REFERENCES

[1] H. van Suchtelen, *Electronics Application Bulletin*, 1952, Vol. 13, p. 88.
[2] H. van Suchtelen, *Electronics Application Bulletin*, 1952, Vol. 13, p. 109.
[3] F. E. Terman, "Radio Engineer's Handbook", pp. 53 and 61, McGraw-Hill, 1943.
[4] J. R. Wait and D. V. Dickson, Radio Physics Laboratory Report, June 1952, 19-2.
[5] J. R. Wait, *Canad. J. Tech.*, 1953, Vol. 31, pp. 9-14 & 132-9.
[6] R. E. Burgess, *Wireless Engineer*, 1946, Vol. 23, p. 172.

U.H.F. TRIODES

Design for Class C Earthed-Grid Operation

By W. J. Pohl, M.Sc. and D. C. Rogers, A.M.I.E.E.

(Standard Telephones & Cables, Ltd., Ilminster, Somerset)

SUMMARY.—The relationships between earthed-grid class C triode performance and electrode dimensions are outlined and combined with the factors concerning the safe operation of the grid. This leads to a simple design procedure which enables the rapid determination of the main electrode dimensions to satisfy given circuit requirements.

The method is applicable to cases in which the maximum permissible grid dissipation can be estimated in terms of the grid dimensions. It applies particularly to disc-seal triodes in which at least one end of each grid wire is in intimate thermal contact with some well-cooled connector external to the valve, which enables a fairly accurate prediction of grid-wire temperature distribution to be made.

1. Introduction

IN the design of u.h.f. triodes for class C operation, the aim is generally to produce a type which will find the greatest variety of uses. In most cases, however, the valve must also satisfy a primary requirement in some specific application and, in this connection, certain features will be of particular importance. For instance, it may be desirable to keep the anode voltage below a certain maximum determined by economic considerations, or a particularly high gain may be wanted. Such features, together with the desired level of drive and output power, will form the starting point of the design. It is usually necessary to find a good compromise between two conflicting requirements. These are:—

(a) The need for small grid pitch and large grid–anode spacings to achieve a high μ, which leads to thin grid wires.

(b) The need for small grid–anode spacings and large grid pitch to avoid excessive grid currents and grid-wire temperatures, which cause a loss of gain, primary grid emission, and grid-wire buckling.

The usual method of attack is to make a tentative estimate of the static characteristics required, and calculate the principal dimensions of the electrodes. From these, skeleton curves of grid and anode currents are derived which enable class C calculations to be carried out. Modifications can then be made until the design appears capable of the desired performance. Not only is this procedure tedious, but there is also a tendency to treat the all-important aspect of grid dissipation as a matter of secondary importance. What is needed is a design system in which the interdependence of earthed-grid class C triode performance, electrode dimensions, and factors concerning the safe operation of the grid is clarified. In this treatment, simplifications in the class C earthed-grid calculations and in the method of calculating grid dissipation are shown to lead to a simple design procedure which will rapidly indicate what can be done within a given framework of conditions. The method gives an accuracy adequate for most practical purposes; it is also easily adapted for frequency-multiplier applications, although this is not demonstrated in this paper.

MS accepted by the Editor, February 1954

LIST OF SYMBOLS

i_k = Total space current
I_k = Peak instantaneous space current
I_g = Peak instantaneous grid current
I_a = Peak instantaneous anode current
V_g = Peak instantaneous grid voltage relative to the cathode
V_a = Minimum instantaneous anode voltage relative to the cathode
l_g = Grid-to-cathode distance measured to the centres of the wires
l_a = Grid–anode spacing measured to the centres of the grid wires
d = Diameter of grid wires
p = Pitch of grid wires
A = Area of cathode
W_g = Total grid dissipation
$W_{g(sp)}$ = Specific grid loading $= W_g p/Ad$
I_{1a} = Crest value of the fundamental-frequency component of anode current
I_{1g} = Crest value of the fundamental-frequency component of grid current
E_b = Direct anode-supply voltage
η = Anode efficiency
ϕ = Grid current flow angle
L = Length of longest grid wire over cathode
k = Thermal conductivity of grid-wire material
τ = Residual tension in grid wire
α = Coefficient of thermal expansion of grid wire
Y = Young's modulus of grid wire
V_{HF} = Peak of anode voltage swing

2. Formulae for Valve Characteristics

(a) A widely-used relationship for the total space current is

$$i_k = \frac{2{\cdot}34 \times 10^{-6}\,(V_g + V_a/\mu)^{3/2}\,A}{\left[l_g + \dfrac{l_g + l_a}{\mu}\right]^2} \qquad (1)$$

Under class C conditions at the crest of the positive excursion of the grid voltage,

$$I_k = \frac{2{\cdot}34 \times 10^{-6}\,(V_g + V_a/\mu)^{3/2}\,A}{\left[l_g + \frac{l_g + l_a}{\mu}\right]^2} \qquad (1a)$$

In practice $V_g \gg V_a/\mu$ and $l_g \gg (l_g + l_a)/\mu$, so that we may write

$$I_k = \frac{2{\cdot}34 \times 10^{-6}\,(V_g)^{3/2}\,A}{{l_g}^2} \qquad (1b)$$

(b) An approximate expression for the grid current is derived as follows:—

I_k = constant $\times\ I_g\sqrt{(V_a/V_g)}$

This is an often-quoted empirical relationship.

Now when

$$\frac{V_g}{V_a} = \left[\frac{l_g}{l_g + l_a}\right]^{4/3}, \quad \frac{I_k}{I_g} \approx \frac{p}{d}$$

hence the constant is $\frac{p}{d}\left[\frac{l_g}{l_g + l_a}\right]^{2/3}$ or

approximately $\frac{p}{d}\left(\frac{l_g}{l_a}\right)^{2/3}$ .. .. (2)

Hence

$$I_g = I_k \frac{d}{p}\left(\frac{l_a}{l_g}\right)^{2/3}\left(\frac{V_g}{V_a}\right)^{\frac{1}{2}} \qquad (3)$$

This approximate relationship has been chosen for its simplicity in preference to other more complex relations published (references 2 and 5).

(c) For the calculation of amplification factor, we use

$$\mu = \frac{l_a/p - \Delta}{T}$$

where Δ and T are functions given in reference 3.

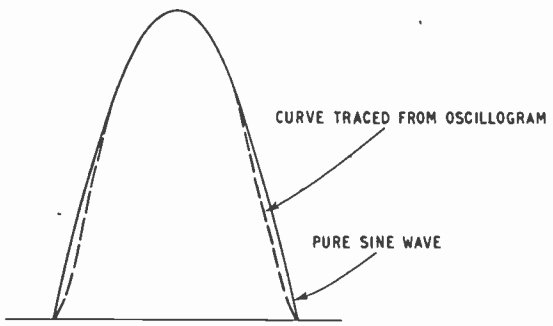

Fig. 1. *Experimental grid-current waveform compared with pure sine wave. The waveform was traced from an oscillogram, showing grid current of 2C39A valve for 120° flow angle, $V_a/E_b = 0{\cdot}1$, $E_b = 350$ volts.*

3. Specific Electric Grid Loading

In the design of electrode spacings it is proposed to make use of the concept of specific electric grid loading, which we define as the power received by the grid divided by the area of the grid wires projected on the cathode. The grid dissipation is given by the product of the instantaneous grid voltage v_g (relative to cathode) and current i_g over the whole cycle; it therefore depends on the grid flow angle. For class C conditions this is usually about 120°, and this figure will be taken as representative.

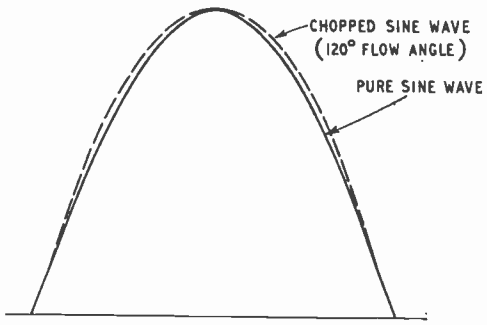

Fig. 2. *Chopped sine wave (120° flow) compared with a pure sine wave, both curves having the same amplitude and base.*

The accurate expressions for the product $v_g \times i_g$ are involved. For the purpose of calculating grid dissipation it is convenient to regard the waveform of v_g and i_g as pure half-sine waves of amplitude V_g and I_g. The dissipation may then easily be determined in terms of V_g and I_g. This simplification may at first sight seem somewhat drastic. Inspection, and also experiment, however, show that it gives a surprisingly good approximation for all flow angles. Fig. 1 shows an oscillogram of grid current of the 2C39A disc-seal triode, taken at 50 c/s for typical operating conditions, together with a half-sine wave having the same amplitude and base. Fig. 2 shows a 120° grid-voltage waveform, together with a half-sine wave of the same amplitude and base. It is seen that for the calculation of mean power the simplification introduces negligible error; the slight error in the grid-current wave is, in fact, partially compensated by an opposite error in the voltage wave. On this basis the total grid dissipation is then

$$W_g = \frac{2}{\pi}\frac{\phi}{2\pi}\int_0^{\pi/2} V_g \sin\theta \times I_g \sin\theta\, d\theta$$

$$= \frac{\phi}{4\pi} V_g I_g$$

Eliminating I_g, using equations (3) and (1b)

$$W_g = 2{\cdot}34 \times 10^{-6}\,\frac{\phi}{4\pi}\,\frac{Ad}{p}\,\frac{{l_a}^{2/3}}{{l_g}^{8/3}}\,\frac{{V_g}^3}{{V_a}^{\frac{1}{2}}} \qquad (5)$$

Therefore, for a 120° flow angle

$$W_g\,(sp) = 0{\cdot}39 \times 10^{-6}\,\frac{l_a}{l_g^{8/3}}\,\frac{V_g^3}{V_a^{\frac{1}{2}}} \quad .. \quad (6)$$

This equation clearly demonstrates the relative effect of the electrode spacings and voltages on the grid loading. The flow angle affects only the constant in the equation.

4. Class C Earthed-Grid Relations

The power output of a class C amplifier is

$$P_{out} = \frac{V_{HF}\,I_{1a}}{2} \quad .. \quad .. \quad .. \quad (7)$$

This includes the 'feed-through power'.
Here $I_{1a} = R_1 I_a$ is the peak value of the fundamental component of anode current.

The d.c. input power is $E_b I_{dc} = E_b R_2 I_a$, where the values of the constants R_1 and R_2 are given in terms of the angle of anode current flow in reference (1). For most cases an angle of 140° will give the best compromise between adequate output power and efficiency, and this value will therefore be taken as representative.* The corresponding values of R_1 and R_2 are 0·44 and 0·25 respectively, so that

$$P_{out} = 0{\cdot}22\,I_a(E_b - V_a) \quad .. \quad .. \quad (8)$$

and

$$P_{dc} = 0{\cdot}25\,E_b\,I_a \quad .. \quad .. \quad (9)$$

giving the anode efficiency

$$\eta = \frac{0{\cdot}22\,(E_b - V_a)}{0{\cdot}25\,E_b} \quad .. \quad .. \quad (10)$$

So the peak anode voltage swing

$$E_b - V_a = \eta\,\frac{0{\cdot}25}{0{\cdot}22}\,E_b = 1{\cdot}135\eta E_b;$$

e.g., for $E_b = 1{,}000$ V, $\eta = 0{\cdot}8$,
$V_a = 0{\cdot}1$, $E_b = 100$ V.

It should be remembered that η is the calculated efficiency and does not include conductor losses in the valve and the circuit.

V_g can now be related to the drive power available. For an earthed-grid amplifier, the drive power is

$$P_{drive} = V_{drive}\left(\frac{I_{1g}}{2} + \frac{I_{1a}}{2}\right)$$

$$= V_{drive}\,\frac{I_{1k}}{2} \approx V_{drive} \times 0{\cdot}22\,I_k$$

$$= (V_g + V_{bias}) \times 0{\cdot}22\,I_k$$

An expression for grid-bias voltage is given in reference (1), which, for a 140° anode flow angle, becomes

$$V_{bias} = \frac{E_b}{\mu} + \left(V_g + \frac{V_a}{\mu}\right)0{\cdot}5$$

Hence the drive power is

$$P_{drive} = 0{\cdot}22\,I_k\left[\frac{E_b}{\mu} + 1{\cdot}5\,V_g + 0{\cdot}5\,\frac{V_a}{\mu}\right]$$

$$\approx 0{\cdot}22\,I_k\left[\frac{E_b}{\mu} + 1{\cdot}5V_g\right] \quad .. \quad .. \quad (11)$$

5. Design Considerations

In the following we shall assume that it is desired to design a valve having a given output power at a stipulated anode efficiency, d.c. supply voltage, and flow angle. We shall assume the efficiency to be 0·8, the grid flow angle 120°, and the anode flow angle 140°. These conditions are typical of normal class C amplifier operation. The method may be carried out with equal facility for other values of efficiency and flow angles. The first step is to obtain the peak instantaneous space current and, in order to do so, one must consider what fraction of the space current will be intercepted by the grid. A high grid current leads to grid-overheating problems, and also to wasted driving power and consequent loss of gain. This may be demonstrated by obtaining from the equations for output and drive power [equations (8) and (11) respectively] an expression for the gain. This is seen to be proportional to I_a/I_k which may be called the 'gain-reduction factor'. It is unity when the grid current is negligible. If high currents are to be avoided, however, the electrode geometry requirements lead to low values of amplification factor and hence also to a loss of gain. Experience with a number of tentative designs has shown that a broad optimum exists in the neighbourhood of $I_a/I_k = 0{\cdot}7$, and this value will be assumed henceforth. Using the design procedure outlined below, it is, in any case, a simple matter to check rapidly whether or not other values will give higher gains in any given design. With I_a/I_k decided upon, I_k is found and, from the maximum permissible current densities for oxide-coated cathodes, the minimum cathode area is determined. At high frequencies the capacitances (and hence the circuit Q factors) should be kept to a minimum, and so it is desirable that the cathode area should also be a minimum. It may, however, be decided to have a greater cathode area for the sake of an improved gain, or in order to obtain longer life with lower current densities. In that case such advantages must be weighed against the disadvantages of increased capacitances which will become of increasing importance with higher frequencies. It will be found that, for a fixed cathode–grid spacing and grid safety factor, the gain varies relatively slowly with the cathode area.

Next, the grid–cathode spacing is decided upon. It is determined from mechanical and economic considerations and should be made as small as practicable. V_g, the peak instantaneous

* Other conditions may be used with equal facility.

grid voltage, can then be determined from equation (1b):

$$V_g = \left[\frac{l_g^2 I_k}{2{\cdot}34 \times 10^{-6} A}\right]^{2/3}$$

At this stage the drive power can be calculated. It is given by equation (11).

$$P_{drive} = 0{\cdot}22\, I_k \left\{\frac{E_b}{\mu} + 1{\cdot}5\left[\frac{l_g^2 I_k}{2{\cdot}34 \times 10^{-6} A}\right]^{2/3}\right\} \quad .. \quad .. \quad .. \quad .. \quad (11a)$$

This equation shows how the drive power, and hence the gain, depends on the ratio l_g^2/A, and indicates that small grid–cathode spacing and large cathode areas are conducive to high gain. It will be found that the drive power depends only to a small extent on μ, so that a reasonable guess for μ will suffice, and enable an estimate of drive power to be made. It is at this stage that preliminary adjustments to the cathode area may be made to meet the gain requirements.

The next step is to determine values of l_a and d such that the permissible grid loading is not exceeded. This is done by obtaining two equations for l_a and d, one based on the electrical characteristics and the other on the grid loading. The specific grid loading can be directly related to wire diameter. In the case of planar structures with tensioned grid wires, it has been shown[4] that for a single wire of length L and diameter d the maximum dissipation before buckling commences is given by

$$W = \frac{3k\tau d^2\pi}{\alpha Y L} \quad .. \quad .. \quad .. \quad (12)$$

This corresponds to a specific grid loading

$$\frac{3\pi k\tau}{\alpha Y L^2} \times d = C_2 \times d, \text{ say} \quad .. \quad (13a)$$

where C_2 is a constant $= \dfrac{3\pi k\tau}{\alpha Y L^2}$

In this case, L is the diameter of the cathode. The other constants are given in the appendix.

Alternatively, where it is feared that grid emission may be troublesome before buckling commences, if t is the maximum permissible temperature of the wire above that of its supporting frame or ring, then

$$C_2 = 2\pi kt/L^2 \quad .. \quad .. \quad .. \quad (13b)$$

In cases where the heat is entirely conducted in one direction, as in some cylindrical structures

$$C_2 = \pi kt/2L^2 \quad .. \quad .. \quad .. \quad (13c)$$

On a gold-plated molybdenum grid, grid emission can become troublesome when the temperature of the hottest parts of the grid wires exceeds 400°C. This figure is based on grid-emission measurements on a tube with a planar grid, in which the maximum grid-wire temperature can be calculated from the measured grid dissipation with a reasonable degree of accuracy[4]. In this valve the grid frame ran at approximately 100°C, giving a recommended figure of 300° for t. For an unplated molybdenum wire grid the figure is considerably lower. It must be remembered that grid emission is greatly influenced by pumping and processing methods which can affect the amount of barium deposited on the grid wires. The subject must be regarded as a rather variable factor which finally requires careful experimental investigation.

The grid pitch p must now be fixed. It is usually desired to make this as large as possible; the grid-wire diameter may then be large in order to keep the grid temperature low. The limit to the pitch is set by 'island effects' which give high negative cut-off voltages. For this reason p must not be greater than about $1{\cdot}8 \times l_g$. It will be seen later that there is no advantage in choosing smaller values of p.

V_g and l_g can now be inserted into equation (6) giving an equation of the form

$$W_{g(sp)} = C_1 (l_a)^{2/3}$$

where $$C_1 = 0{\cdot}390 \times 10^{-6} \frac{V_g^3}{l_g^{8/3} V_a^{1/2}}$$

This may now be related to equation (13a) or (13b) or (13c)

$$F \times W_{g(sp)} = C_2 d$$

where F is a suitable safety factor.

$$FC_1 (l_a)^{2/3} = C_2 d \quad .. \quad .. \quad .. \quad (14)$$

A second equation is obtained from the fact that we have stipulated that the gain reduction factor $I_a/I_k = 0{\cdot}7$

$$\frac{I_a}{I_k} = 1 - \frac{d}{p}\left(\frac{l_a}{l_g}\right)^{2/3}\left(\frac{V_g}{V_a}\right)^{\frac{1}{2}} = 0{\cdot}7 \quad \text{from (3)}$$

Hence $$K_1 d\,(l_a)^{2/3} = 0{\cdot}3 \quad .. \quad .. \quad .. \quad (15)$$

where $$K_1 = \frac{1}{p\, l_g^{2/3}}\left(\frac{V_g}{0{\cdot}1E_b}\right)^{\frac{1}{2}}$$

and, for $\eta = 0{\cdot}8$, $V_a = 0{\cdot}1E_b$

Equations (14) and (15) are solved simultaneously for d and l_a

$$l_a = \left(\frac{0{\cdot}3\, C_2}{K_1 F C_1}\right)^{3/4} \quad .. \quad .. \quad .. \quad (14a)$$

$$d = \sqrt{\left(\frac{0{\cdot}3\, FC_1}{K_1 C_2}\right)} \quad .. \quad .. \quad (15a)$$

At this stage μ is calculated, using, for example, Ollendorff's table[3], and the gain must be recalculated by the use of equation (11). If the gain is not satisfactory, adjustments must be made to the cathode area.

6. Adjustment of the Cathode Area

It is a straightforward matter to show from the foregoing equations that if the cathode area is changed in a given design, then, to maintain the

same output power, anode efficiency, grid safety factor, and gain reduction factor,

$$d \propto 1/A^{1/3} \quad .. \quad .. \quad .. \quad .. \quad (16)$$

$$l_a \propto A \quad .. \quad .. \quad .. \quad .. \quad (17)$$

These relations enable new values of d and l_a to be found when the cathode area is adjusted to meet gain requirements. This is illustrated in the example.

7. Transit-Time Effects

It may also be asked whether transit-time considerations should play a part in the choice of l_a. This question has received considerable attention from theoreticians, but no practical results have been published in which the cause for the loss of efficiencies at high frequencies can be distinctly differentiated into transit-time and ohmic-loss effects. The writers have made circuit Q measurements of cavities for the 2C39A valve at 2,300 Mc/s. At this frequency the valve works with an efficiency of only 20% or so at $E_b = 500$ V. The measured Q, however, accounts largely for the loss of efficiency, even though the transit-times are comparable with the duration of one cycle. At 1,000 Mc/s the valve gives an efficiency of 50% as an oscillator. One may conclude, therefore, that circuit-loss considerations must be the focus of the designer's attention. Although the transit-time in the grid–anode space is proportional to l_a, so, approximately, is the circuit Q, and misgivings concerning large values of l_a must be weighed against this.

If Q_L is the Q factor of a loaded cavity, loading being such that the valve has its maximum efficiency, and Q_0 is the Q factor of the unloaded cavity, then the cavity efficiency is given by

$$\eta_c = \frac{Q_0 - Q_L}{Q_0} = \frac{\text{Useful power in load}}{\text{Total r.f. power}}$$

8. Summary of Design Procedure

We are now in a position to summarize the design procedure. The constants given apply to an anode flow angle of 140°, a grid flow angle of 120° and an anode efficiency of 0·8. The gain reduction factor I_a/I_k is taken as 0·7.

(i) From the output required, calculate I_a. [Equs. (8), (9) and (10)]

(ii) Calculate I_k from $I_a/I_k = 0{\cdot}7$.

(iii) Decide on the minimum cathode area A. For c.w. operation and 800°C, $I_k/A = 7{\cdot}0$ A/sq. in. max.

(iv) Decide on the grid–cathode spacing l_g. This should be as small as mechanical and economic considerations permit.

(v) Decide on the grid pitch, p. This should be approximately $1{\cdot}8\ l_g$. Find V_g from equation (1b).

(vi) Find C_2, C_1 and K_1.

For planar structures with circular apertures,

$$C_2 = \frac{3\pi k\tau}{\alpha Y L^2} \text{ or } \frac{2\pi tk}{L^2} \text{ or } \frac{\pi tk}{2L^2}$$

$$C_1 = \frac{0{\cdot}390 \times 10^{-6}\, V_g^3}{l_g^{8/3}\,(0{\cdot}1\,E_b)^{\frac{1}{2}}}$$

$$K_1 = \frac{1}{p l_g^{2/3}}\left(\frac{V_g}{0{\cdot}1\,E_b}\right)^{\frac{1}{2}}$$

(vii) Find l_a and d.

$$d = \sqrt{\left(\frac{0{\cdot}3\,FC_1}{K_1 C_2}\right)}; \quad l_a = \left(\frac{0{\cdot}3C_2}{K_1 FC_1}\right)^{3/4}$$

(viii) Find μ from Ollendorff's tables, and calculate the drive power from equation (11). (See ref. 3.)

(ix) If the gain is insufficient, increase A. Find the new value of d and l_a by the use of equations (16) and (17). Find μ and the drive power from equation (11).

Example

Let a valve be designed for a nominal output of 40 W, at a direct voltage of 600 V. If conductor losses are estimated at 20% the valve should be calculated to give an output power of 48 W, at an anode efficiency of, say, 0·8. If the grid–cathode spacing is fixed at, say, 0·004 in. and the maximum permissible peak cathode-current density is taken at 6·5 A per sq/in., then, if we follow the design procedure for a molybdenum wire grid on a circular frame, using the appropriate values of α, Y and τ given in the appendix, we obtain the designs of Table 1 for different values of safety factor F:

TABLE 1

F Safety factor	d (in. × 10^{-3})	l_a (in. × 10^{-3})	d/p	μ	Drive power (watts)
2	0·855	43	0·129	44	4·5
3	1·05	32	0·162	40·7	4·6
4	1·21	25·5	0·186	40·2	4·7
5	1·35	21·5	0·208	40·2	4·7
8	1·71	15	0·263	40·3	4·4
10	1·98	13	0·304	47	4·3
12	2·09	11·2	0·322	49	4·2
15	2·34	9·4	0·360	57	3·8
20	2·7	7·6	0·414	72·5	3·5

This shows that it is not worth while skimping the safety factor of the valve for the sake of an improved gain, although the aspect of sparkover in choosing l_a must also influence the choice of F. It will be seen that high values of F give too small a grid–anode spacing.

We shall fix on a safety factor of 10 which gives an l_a of 13×10^{-3} in., this being as close as is permissible for 600-V operation, and examine what happens when we increase the area of the cathode, thereby decreasing the current density.

In equations (16) and (17) we have shown that if A is increased by a factor m, say $(m > 1)$, d may be decreased by a factor $1/m^{1/3}$ and l_a may be increased by a factor m. V_g is decreased by $1/m^{2/3}$. The results are shown in Table 2.

The gain is not proportional to the area, and considerable increases in area may be required to give small improvements in gain. Considerations outlined in section 7 must be given due weight in this connection.

TABLE 2

m	A (sq. in.)	V_g (volts)	d (in. $\times 10^{-3}$)	l_a (in. $\times 10^{-3}$)	d/p	μ	Drive power (watts)
	0·09	12	2·0	13·0	0·304	47·0	4·3
1·1	0·099	11·3	1·94	14·3	0·298	51·0	4·1
1·2	0·108	10·6	1·89	15·6	0·290	52·0	3·9
1·3	0·117	10·1	1·83	16·9	0·282	53·0	3·75
1·4	0·126	9·6	1·78	18·2	0·274	54·5	3·65
1·5	0·135	9·15	1·75	19·5	0·269	57·0	3·45
1·75	0·158	8·25	1·66	22·8	0·257	60·0	3·16
2·0	0·18	7·6	1·59	26·0	0·244	61·0	3·02

Acknowledgments

The authors are indebted to Messrs. Standard Telephones & Cables, Ltd., for permission to publish this paper.

APPENDIX

PROPERTIES OF GRID-WIRE MATERIALS

Calculation of $C_2 = \dfrac{3\pi k\tau}{\alpha Y L^2}$ for planar structures with circular grid apertures.

(1) *For molybdenum wire:*

$k = 1{\cdot}5$ W/cm/°C. $= 3{\cdot}8$ W/in./°C.

τ may be taken as the yield point of grid wire at 400°C.

$\tau \approx 30$ kg/mm².

$\alpha = 5{\cdot}7 \times 10^{-6}$.

$Y = 26{\cdot}4 \times 10^3$ kg/mm².

(This figure is representative for diameters in the region of 0·002 in. There is a slight variation with diameter.)

This gives $C_2 = 7{\cdot}15/L^2$ W/in. $\times 10^{-3}$/°C.

(2) *For tungsten wire:*

k (at 300°C) $= 1{\cdot}3$ W/cm/°C $= 3{\cdot}3$ W/in./°C. The yield point τ for tungsten is $12{\cdot}0 \times 10^4$ gm/mm² at 325°C (measured on 0·001-in. diameter wire). This is not attainable without especially powerful tensioning and it is safer to take a figure of $6{\cdot}0 \times 10^4$ gm/mm².

Y = approximately 30×10^3 kg/mm².

$\alpha = 4{\cdot}44 \times 10^{-6}$.

Hence $C_2 = 14{\cdot}2/L^2$ W/in. $\times 10^{-3}$/°C.

Note: As shown in Table 3, Young's modulus is a function of wire diameter.

TABLE 3

Wire dia. in. $\times 10^{-3}$	Y in kg/mm²
6	26,000
4	31,500
2	33,200
1	34,000

REFERENCES

[1] Terman, "Radio Engineering", p. 325 *et seq.*

[2] G. Wood, "Positive Grid Characteristics of Triodes", *Proc. Inst. Radio Engrs*, June 1948, p. 804.

[3] Fremlin, Hall and Shatford, "Triode Amplification Factors", *Electrical Communication*, Dec. 1946.

[4] W. J. Pohl, "Aspects in the Design and Manufacture of Grids for U.H.F. Triodes", *Electronic Engineering*, March 1951.

[5] K. Spangenberg, "Current Division in Plane Electrode Triodes", *Proc. Inst. Radio Engrs*, May 1940, p. 226.

FARADAY MEDAL AWARD

The Council of the Institution of Electrical Engineers has awarded the Faraday medal to "Sir John Cockcroft, K.C.B., C.B.E., M.A., M.Sc.Tech., Ph.D., F.R.S., M.I.E.E., Director of the Atomic Energy Research Establishment, Harwell, for the conspicuous services he has rendered to the advancement of electrical science, for his distinguished work in the field of nuclear physics and the development of power from nuclear sources".

NEW YEAR HONOURS

Among those receiving decorations in the New Year Honours List are :—

C.M.G.

R. C. McCall, British Broadcasting Corporation.

O.B.E.

J. Clarricoats, Radio Society of Great Britain.

V. M. Roberts, British Thomson-Houston Co. Ltd.

EXHIBITIONS

The National Radio Show will be held this year at Earls Court, London, from 24th August to 3rd September, with a preview for overseas visitors on 23rd August.

The Northern Radio Show will be held at the City Hall, Manchester, from May 2nd to 14th.

The British Instrument Industries' Exhibition will be held at Earls Court, London, from 28th June to 9th July.

The British Plastics Exhibition will be held at Olympia, London, from June 1st to 11th.

SHUNT-DIODE RECTIFIER IN VOLTAGE MEASUREMENT

Effect of Source Resistance on Efficiency of Rectification

By M. G. Scroggie, B.Sc., M.I.E.E.

Introduction

THE quasi-linear operation of the diode rectifier has frequently been analysed, but attention is usually confined to the series form of circuit[1–7], Fig. 1. For some purposes it is more convenient to adopt the shunt form, Fig. 2, which in several respects is different, so that the conclusions drawn for the series circuit do not necessarily apply to it. One important distinction, of course, is the position of the capacitor C, which in Fig. 2 excludes the z.f. component, allowing the diode to be used for measuring an alternating voltage regardless of any fixed p.d. that may also be present in the source of the voltage, and without the necessity for making sure that a continuous d.c. path exists. At the same time it allows the cathode and heater, and also one terminal of the source, to be connected to an earthy point in the circuit without introducing an undesirable admittance across the load resistance R or the diode. This arrangement is therefore much used in valve voltmeters. It also occurs in one of the two forms of leaky-grid detector, but as that is now seldom used, at least at a sufficient input voltage level to be regarded as substantially linear, it is not specifically in view in the present analysis, which moreover is confined to unmodulated inputs, and is therefore chiefly applicable to valve voltmeters.

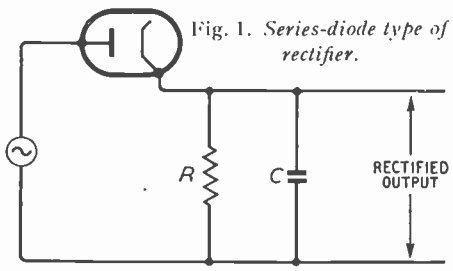

Fig. 1. *Series-diode type of rectifier.*

As a result of C in Fig. 2 being in series with, instead of shunted across, R, nearly the whole of the input voltage is found across R along with the rectified (z.f.) component. Since the output is usually fed into an amplifier, where the presence of such a large ripple is in general undesirable, some sort of simple filter is almost invariably interposed. It usually takes one or other of the forms shown in Figs. 3 and 4. To some extent the rectification process is affected by the form and circuit parameters of the filter, so for measuring apparatus especially it is desirable to take these into account.

The main object of the present inquiry is to extend to Figs. 2–4 the results already known for Fig. 1, as regards the effect on the ratio of rectified output voltage to peak input voltage of the ratio of series resistance to load resistance[1,3,6,7]. A non-mathematical account has been given elsewhere by the present author[10].

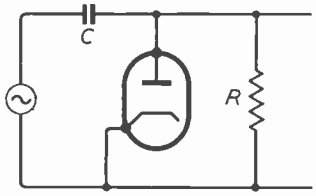

Fig. 2. *Shunt-diode type of rectifier.*

The following assumptions will be made:

(1) That the source is, or can be converted by Thévenin's theorem into, an e.m.f. $E_{max}\cos\omega t$ in series with a resistance R_s.

(2) That the resistance of the diode with anode negative is infinite, and with anode positive is either zero or a constant finite quantity. (This is approximately true when R is of the megohm order and E_{max} is at least several volts, and when the initial or intercept voltage has been balanced out by one of the usual means[9].)

(3) That the reactance of C (or C_1 and C_2) at the working frequency is negligible (i.e., $fCR \approx \infty$), so that the potentials across the capacitors do not vary during the cycle. (But the effect of finite fCR will later be briefly considered.)

(4) That there is no load admittance other than shown in Figs. 1–4. (This assumption implies that the rectifier works into an amplifier with negligible grid current[8].

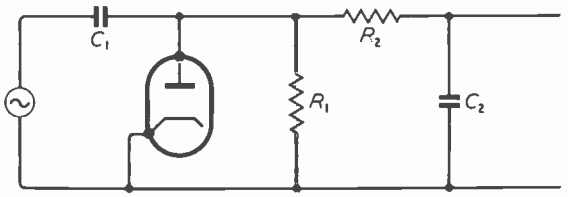

Fig. 3. *Shunt-diode rectifier with simple ripple filter (first type).*

MS accepted by the Editor, March 1954

'Rectifier' means the whole combination as, for example, in Figs. 1–4, less the voltage source and its impedance.)

Series-Diode Circuit

With these assumptions the operation of the series circuit (Fig. 1) can be illustrated as in Fig. 5. The whole cycle, $-\theta$ to $2\pi - \theta$, can be divided into the diode conducting epoch, $-\theta$ to $+\theta$, when C is being charged through R_c $(= R_s + R_d)$ and the non-conducting epoch, θ to $2\pi - \theta$. C is discharging through R at a constant rate throughout the cycle. A sufficient sample of the cycle's operations is contained in the half-cycle 0 to π.

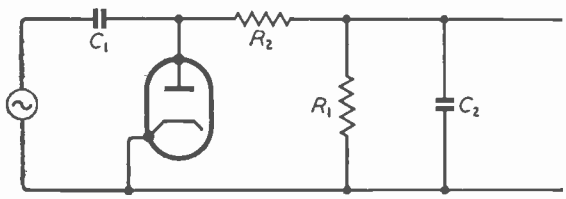

Fig. 4 (above). *Shunt-diode rectifier with simple ripple filter (second type).*

Fig. 5 (below). *Symbols used in discussing Fig. 1 circuit, and potential diagram.*

Fig. 6 (right). *Calculated graph of efficiency of rectification (η) of Fig. 5 circuit as a function of the ratio of series resistance to load resistance. Measured points in the Fig. 5 circuit are marked X; those in Fig. 9, O.*

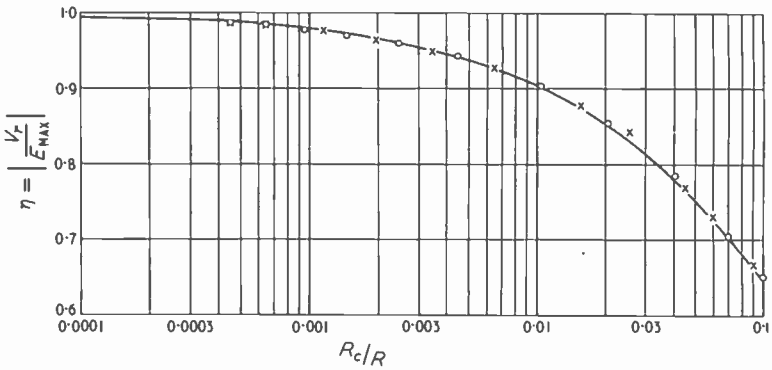

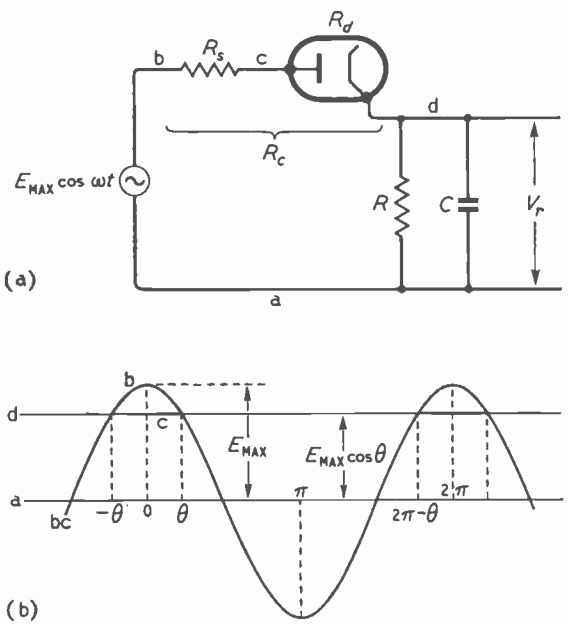

V_r, the z.f. output, is unaccompanied by any other component and is obviously equal to $E_{max} \cos \theta$. It has been shown[6] that

$$\frac{R_c}{R} = \frac{2 \sin \theta - 2\theta \cos \theta}{2\pi \cos \theta}$$

which can more conveniently be written

$$\frac{R_c}{R} = \frac{\tan \theta - \theta}{\pi} \quad .. \quad .. \quad .. \quad (1)$$

It is therefore easy to plot the efficiency of rectification, η, $= | V_r/E_{max} | = \cos \theta$ against R_c/R (Fig. 6). For valve voltmeters one is particularly interested in the 'error', $1 - \eta$ expressed as a percentage, for smaller values than are shown clearly in Fig. 6. Fig. 7 is therefore an expansion of the upper part of Fig. 6, scaled in percentage error. An error of 1% corresponds to $\theta = 8{\cdot}1°$, or a total conduction angle of 16·2°; and as the angle is reduced the difference between θ and $\tan \theta$, and consequently R_c/R, rapidly becomes extremely small.

The minimum realizable value of R_c is, of course, the forward resistance of the diode, R_d. The fact that as the current approaches zero R_d rapidly rises is a main cause of the familiar bottom bend. Under the nearly linear conditions assumed, most diodes have a forward resistance of a few hundred ohms, sufficient, with R of the order of 1 MΩ, to make V_r something like 1% less than E_{max}; but this can hardly be described as an error, for it would be discounted in the calibration. The effective error is really $1 - \eta/\eta_0$, where η_0 is the value of η with no source resistance (i.e., $R_s = 0$). The greater the diode resistance R_d, the less the effect R_s has on V_r.

Diode resistance is therefore beneficial in stabilizing the rectifier against the effects of source resistance, and it is interesting to see what benefit can be obtained from artificially increasing it by resistance in series. In Fig. 8 the ratio of R_s to R causing the error $1 - \eta/\eta_0$ to be 1% is

plotted against R_d/R, R_d being the resistance of the diode plus any other series resistance incorporated in the rectifier circuit. The starting point, $R_d = 0$ ($\eta_0 = 1$), is at $R_s/R = 0{\cdot}00031$, and with a low-resistance diode and $R = 10$ MΩ or more the figure would not be much greater. If, however, sufficient resistance were added to

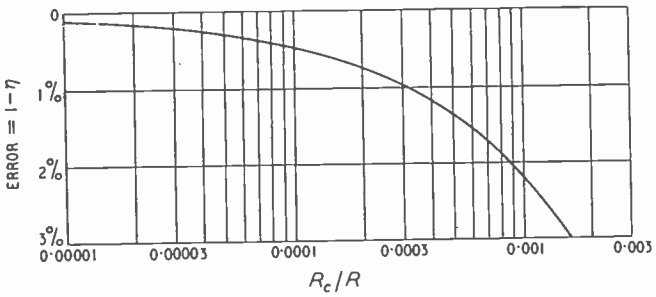

Fig. 7. *Enlargement of the top portion of Fig. 6, to a scale of $1-\eta$ as a percentage.*

make $\eta = 1/\sqrt{2}$, so that V_r would conveniently be equal to E_{rms}, R_s/R for 1% error would be 0·0031—10 times greater. Moreover the larger resistance ($= 0{\cdot}068R$) added to the diode would greatly improve its linearity. On the other hand, these benefits might not be considered to be worth the serious reduction of upper frequency limit imposed by the undesirable effects of such a resistance in association with circuit capacitances, unless only low-frequency measurements were in view. It is at audio frequencies that errors of the magnitudes that have been considered are most likely to occur; at radio frequencies the position is somewhat different.

The reason for this is that the source is likely to be a tuned circuit, the stored energy of which maintains a sinusoidal waveform despite the extreme inequality of load imposed by the rectifier during the cycle[4,5]. Consequently it is incorrect to regard the dynamic resistance of the tuned circuit as R_s for the purpose of assessing the source-resistance error as heretofore. The relevant quantity is the effective input resistance of the rectifier, R_i; that is to say, the value of ohmic resistance which, if shunted across the tuned circuit, would load it to the same extent as the rectifier. Various approximations have been deduced for this[2,6,7]; in the circuit of Fig. 1 under the conditions assumed it tends to $R/2$ as R_d tends to zero, and this approximation is satisfactory for R_d/R ⩾ about 0·001. An approximation, good up to about 0·03, is $R/2\eta$. These neglect losses, important at high r.f., in stray capacitances, including the diode. By

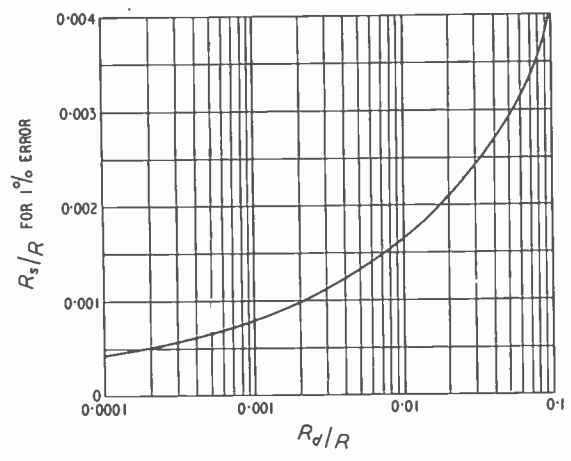

Fig. 8. *Relative source resistance (R_s/R) sufficient to cause 1% error ($1-\eta/\eta_0$) as a function of the relative internal resistance (of the diode, etc.).*

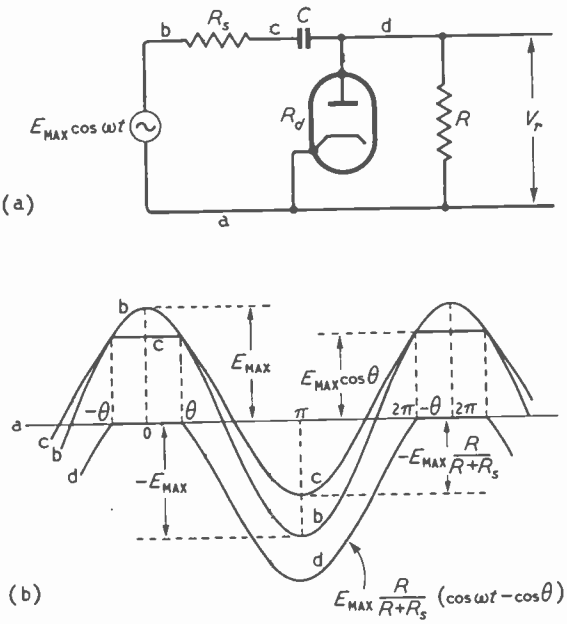

Fig. 9. *Symbols used in discussing Fig. 2 circuit, and potential diagram.*

definition of R_i, the error due to diode rectifier loading is the proportionate reduction in voltage across the tuned circuit when loaded by a resistance equal to R_i. There is, of course, the same liability as before to loss due to series resistance, but this would normally be only R_d, presumably allowed for in the calibration.

Shunt-Diode Circuit

Having recapitulated for Fig. 1, we now turn to Fig. 2, elaborated in Fig. 9. It is assumed for the present that the diode forward resistance, R_d, is zero. When R_s also is zero, R receives not

only the rectified voltage V_r but also the full alternating voltage from the source, so its input resistance R_i in these circumstances is $R/3$. As in the series circuit, C is being charged through R_s from 0 to θ, but its discharge during the half-cycle is confined to θ to π and takes place at a variable instead of a steady rate, through $R_s + R$ instead of through R only. The e.m.f. during both operations is E_{max} (cos ωt − cos θ).

During each half-cycle beginning at 0 the net charge entering C is zero; i.e.,

$$\frac{E_{max}}{\omega R_s}\int_0^{\theta}(\cos\omega t - \cos\theta)\,d\omega t - \frac{E_{max}}{\omega\,(R+R_s)}\int_{\theta}^{\pi}(\cos\omega t - \cos\theta)\,d\omega t = 0 \quad .. \quad (2)$$

Integrating

$$(R + R_s)(\sin\theta - \theta\cos\theta) = R_s\,(\sin\theta + \pi\cos\theta - \theta\cos\theta) \quad .. \quad (3)$$

$$R\,(\sin\theta - \theta\cos\theta) = R_s\pi\cos\theta$$

$$\frac{R_s}{R} = \frac{\tan\theta - \theta}{\pi} \quad .. \quad (4)$$

the same as for the series circuit [Equ. (1) when $R_d = 0$]. Since V_r is the mean value of V_{ad}*

$$V_r = \frac{E_{max}R}{\pi(R + R_s)}\int_0^{\pi}(\cos\omega t - \cos\theta)\,d\omega t = \frac{-E_{max}R}{\pi\,(R+R_s)}\,(\sin\theta + \pi\cos\theta - \theta\cos\theta)$$

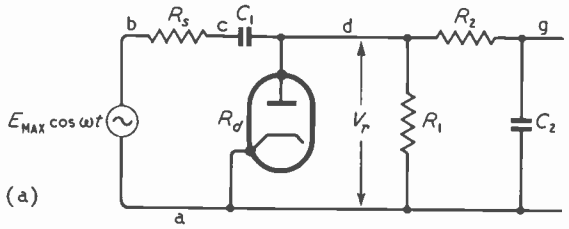

(a)

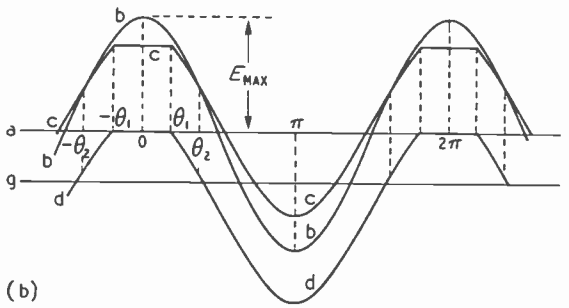

(b)

Fig. 10. *Symbols used in discussing Fig. 3 circuit, and potential diagram.*

* The double-subscript notation for voltages is here used in the sense $V_{ad} = V_d - V_a$, where V_d and V_a are the potentials of points d and a respectively.

Substituting for $R + R_s$ from (3) and then R_s/R from (4) we obtain

$$V_r = -E_{max}\cos\theta$$

Hence

$$\eta = |\,V_r/E_{max}\,| = \cos\theta$$

So as regards R_s/R and η the various differences between the series and shunt circuits cancel out, and the data given in Figs. 6–8 apply also to the shunt circuit, if R_d is neglected.

Effect of Diode Resistance

If now there is appreciable diode resistance (inherent or added) as well as R_s, the conditions from θ to π are the same as before, because R_d is open-circuited; but from 0 to θ the resistance through which C is charged is $R_s + R_dR/(R_d + R)$: call it $R_s + R'_d$. Substituting $R_s + R'_d$ for R_s in the first term of (2) and proceeding as before we obtain

$$(R + R_s)(\sin\theta - \theta\cos\theta) = (R_s + R'_d)(\sin\theta + \pi\cos\theta - \theta\sin\theta) \quad .. \quad (5)$$

from which

$$\frac{R_s + R'_d}{R - R'_d} = \frac{\tan\theta - \theta}{\pi} \quad .. \quad (6)$$

While C is charging, V_{ad} is not zero, but receives a share of the positive peak; so

$$V_r = \frac{E_{max}\,R'_d}{\pi(R_s + R'_d)}\int_0^{\theta}(\cos\omega t - \cos\theta)\,d\omega t + \frac{E_{max}\;R}{\pi(R + R_s)}\int_{\theta}^{\pi}(\cos\omega t - \cos\theta)\,d\omega t$$

$$= \frac{E_{max}}{\pi}\left[\frac{R'_d}{R_s + R'_d}\,(\sin\theta - \theta\cos\theta) - \frac{R}{R + R_s}\,(\sin\theta + \pi\cos\theta - \theta\cos\theta)\right]$$

Substituting for $R + R_s$ from (5) and then $(R_s + R'_d)/(R - R'_d)$ from (6) we obtain

$$V_r = -E_{max}\cos\theta \quad \text{and} \quad \eta = \cos\theta$$

as before.

If $R_s = 0$, $\dfrac{R_s + R'_d}{R - R'_d}$ reduces to $\dfrac{R_d}{R}$. Therefore if the whole of the resistance through which C is charged (i.e., R_c) is R_s *or* R_d, Equ. (1) is exact for the shunt circuit as well as for the series circuit. Even in the more practical case of its being divided between the R_s and R_d positions, it is approximately correct unless R_s and R_d are both large. For if $R_d \ll R$; $R'_d \approx R_d$ and

$$\frac{R_s + R'_d}{R - R'_d} \approx \frac{R_s + R_d}{R} = \frac{R_c}{R}$$

By putting $R_d = R_c - R_s$, and differentiating $\dfrac{R_s + R'_d}{R - R'_d} - \dfrac{R_c}{R} = y$ with respect to R_s and equating to zero it can easily be shown that the maximum y occurs when $R_d = R_s$. Substituting this equality in y, we obtain

$$y_{max} = \frac{R^2_c}{4R^2}$$

and the ratio of this to R_c/R is $R_c/4R$. So unless, for example, R_c/R is greater than 0·1 the error in the evaluation of $\frac{R_s + R'_d}{R - R'_d}$ from putting it equal to R_c/R cannot at worst ($R_d = R_s$) exceed 2·5%, which is insignificant. In other words, not only Fig. 7 but also the whole of Figs. 6 and 8 can be regarded as applicable to both series and unfiltered shunt rectifiers with R_c made up of R_s and R_d in any proportion.

Shunt Circuit with Filter (Fig. 3 Type)

Here there are two critical angles, θ_1 and θ_2. The first, corresponding to θ in the previous cases, at which the diode current and voltage are both zero, occurs when the current i around the circuit 'abcdga' (Fig. 10) brings 'd' to the same potential as 'a', so is defined by

$$E_{max} \cos \theta_1 - iR_s - V_{dc} = V_{ag} + iR_2 = 0$$

Eliminating i we obtain

$$V_{dc} = E_{max} \cos \theta_1 + V_{ag} R_s/R_2$$

θ_2 is the phase at which the current i ceases to flow. Thus

$$V_{dc} = E_{max} \cos \theta_2 - \frac{R_1}{R_1 + R_2} V_{ag} \quad .. \quad (7)$$

Solving for V_{dc} and V_{ag},

$$V_{dc} = E_{max} \frac{R' \cos \theta_1 + R_s \cos \theta_2}{R' + R_s} \quad .. \quad (8)$$

and

$$V_{ag} = E_{max} \frac{R_2 (\cos \theta_2 - \cos \theta_1)}{R' + R_s} \quad .. \quad (9)$$

where $R' = \frac{R_1 R_2}{R_1 + R_2}$

Equating to zero the net charge entering C_1 during the half-cycle beginning at 0,

$$\frac{E_{max}}{\omega R_s} \int_0^{\theta_1} \left(\cos \omega t - \frac{R' \cos \theta_1 + R_s \theta_2}{R' + R_s} \right) d\omega t -$$

$$\frac{E_{max}}{\omega (R' + R_s)} \int_{\theta_1}^{\pi} (\cos \omega t - \cos \theta_2) \, d\omega t = 0$$

Integrating,

$$\left(R' + R_s\right)\left(\sin \theta_1 - \theta_1 \frac{R' \cos \theta_1 + R_s \cos \theta_2}{R' + R_s}\right)$$

$$= R_s(\sin \theta_1 + \pi \cos \theta_2 - \theta_1 \cos \theta_2)$$

$$R'(\sin \theta_1 - \theta_1 \cos \theta_1) = R_s \pi \cos \theta_2$$

$$\frac{R_s}{R'} = \frac{\sin \theta_1 - \theta_1 \cos \theta_1}{\pi \cos \theta_2} \quad (10)$$

V_r is the mean value of V_{ad}:

$$V_r = \frac{E_{max} R'}{\pi (R' + R_s)} \int_{\theta_1}^{\pi} (\cos \omega t - \cos \theta_1) \, d\omega t$$

$$= \frac{-E_{max} R'}{\pi (R' + R_s)} (\sin \theta_1 + \pi \cos \theta_1 - \theta_1 \cos \theta_1) \quad (11)$$

Since this is equal to V_{ag} (9),

$$\frac{R'}{\pi} (\sin \theta_1 + \pi \cos \theta_1 - \theta_1 \cos \theta_1)$$

$$= R_2(\cos \theta_1 - \cos \theta_2)$$

Substituting in (10) the value of $\cos \theta_2$ implicit here, we obtain

$$\frac{R_s}{R_1 + R_s R_1/R_2} = \frac{\tan \theta_1 - \theta_1}{\pi} \quad .. \quad (12)$$

This is in the same form as (4) for comparison; the most convenient form, however, is perhaps

$$\frac{R_1}{R_s} = \frac{\pi}{\tan \theta_1 - \theta_1} - \frac{R_1}{R_2} \quad .. \quad .. \quad (13)$$

In either form it is obvious that if R_2 is made ∞, both circuit and equation reduce to the simple shunt case.

Combining (11) and (13) we obtain

$$\eta = \left| \frac{V_r}{E_{max}} \right| = \left(1 - \frac{R_1}{R_2} \cdot \frac{\tan \theta_1 - \theta_1}{\pi}\right) \cos \theta_1$$

$$= \frac{R_2}{R_2 + R_s} \cos \theta_1 \quad (14)$$

Here again, when $R_2 = \infty$, $\eta = \cos \theta_1$

When R_2 is of the same order of magnitude as R_1, the graph of η against R_s/R_1 differs very appreciably from that for $R_2 = \infty$ (Fig. 6) when the error $1 - \eta$ is large; but for the small values of $1 - \eta$ shown in Fig. 7 the difference is negligible. Fig. 11 shows the equivalent of Fig. 6, with R_2 arbitrarily $= 0{\cdot}54R_1$.

The limiting value of the input resistance R_i as R_s tends to zero is $R_1R_2/(R_1 + 3R_2)$, which, when $R_1 = R_2$, is $R_1/4$.

The addition of the filter, then, by reducing R_i, somewhat increases the load on the source, and also the error, but the increase in error is negligible except when the error is large.

Shunt Circuit with Filter (Fig. 4 Type)

Referring to Fig. 12, at phase θ_1 the situation is the same as with the previous filter; i.e.,

$$V_{dc} = E_{max} \cos \theta_1 + V_{ag} R_s/R_2$$

At θ_2 the only difference is that what in (7) was $\frac{R_1}{R_1 + R_2} V_{ag}$ is now V_{ag}:

$$V_{dc} = E_{max} \cos \theta_2 - V_{ag}$$

From these we obtain

$$V_{dc} = E_{max} \frac{R_2 \cos \theta_1 + R_s \cos \theta_2}{R_2 + R_s}$$

$$V_{ag} = E_{max} \frac{R_2(\cos \theta_2 - \cos \theta_1)}{R_2 + R_s} \quad .. \quad (15)$$

These are the same as (8) and (9) except for R_2 in place of R'. Following the same procedure as before, therefore, we have in place of (10) and (11)

$$\frac{R_s}{R_2} = \frac{\sin\theta_1 - \theta_1\cos\theta_1}{\pi\cos\theta_2} \quad .. \quad .. \quad (16)$$

$$V_r = \frac{-E_{max}R_2}{\pi(R_2+R_s)}(\sin\theta_1 + \pi\cos\theta_1 - \theta_1\cos\theta_1) \quad .. \quad .. \quad .. \quad (17)$$

In this case, however, V_{ag} is not equal to V_r but to $V_r\frac{R_1}{R_1+R_2}$, so from (15) and (17)

$$\frac{R_1}{\pi}(\sin\theta_1 + \pi\cos\theta_1 - \theta_1\cos\theta_1) = (R_1+R_2)(\cos\theta_1 - \cos\theta_2)$$

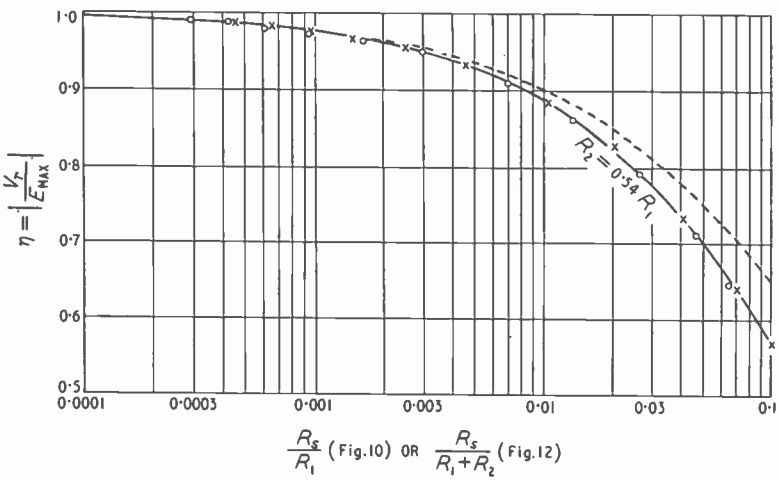

Fig. 11. *The full-line curve is calculated for the Fig.* 10 *and Fig.* 12 *circuits, with* $R_2/R_1 = 0{\cdot}54$. *The Fig.* 6 *curve is dotted in for comparison. Measured points in the Fig.* 10 *circuit are marked* ×; *those in Fig.* 12, ○.

Substituting in (16) the value of $\cos\theta_2$ implicit here, we obtain

$$\frac{R_s}{R_1+R_2+R_sR_1/R_2} = \frac{\tan\theta_1 - \theta_1}{\pi}$$

and

$$\frac{R_1+R_2}{R_s} = \frac{\pi}{\tan\theta_1 - \theta_1} - \frac{R_1}{R_2} \quad .. \quad .. \quad .. \quad .. \quad (18)$$

corresponding to (12) and (13) respectively.

Combining (17) and (18), we obtain

$$\eta = \left(1 - \frac{R_1}{R_2}\cdot\frac{\tan\theta_1 - \theta_1}{\pi}\right)\cos\theta_1 \quad .. \quad (19)$$

$$= \frac{R_1+R_2}{R_1+R_2+R_sR_1/R_2}\cdot\cos\theta_1$$

Circuit and equations are reduced to the simple shunt case by putting $R_1 = 0$.

$R_1 + R_2$ in Fig. 4 takes the place of R_1 in Fig. 3 and R in Figs. 1 and 2 as the diode load resistance. Since (14) and (19) are identical, as are also the right-hand sides of (13) and (18), it is clear that Fig. 11 applies also to this circuit if $R_s/(R_1+R_2)$ is substituted for R_s/R_1 as abscissa, and similarly Fig. 7 is sufficiently accurate to be adapted in the same way. The most important difference, of course, is that the output voltage V_r is reduced in the ratio $R_1/(R_1+R_2)$. This may actually be done deliberately[9] in order that a z.f. valve voltmeter to which the rectifier is prefixed may read r.m.s. values of sinusoidal voltages. There may also be a practical advantage in having R_1 as part of the amplifier.

The limiting value of the input resistance of the rectifier, R_i, as R_s tends to zero, is

$$R_2(R_1+R_2)/(R_1+3R_2).$$

When $R_1 + R_2 = \sqrt{2}R_1$,

$$R_i = \frac{R_1}{3{\cdot}83} = \frac{R_2}{1{\cdot}58} = \frac{R_1+R_2}{5{\cdot}42}$$

In general, since R_2 in this circuit cannot conveniently be made so large as in Fig. 3, the load imposed on the source by this filter is likely to be greater.

Effect of Finite Capacitor Reactance

Provided that C_2 in Figs. 3 and 4 is large enough in conjunction with R_2 for its filtering to be reasonably effective at the lowest frequency (fC_2R_2 say at least equal to 2) its value has very little effect on the rectified voltage. The significant parameter with regard to η is fCR in

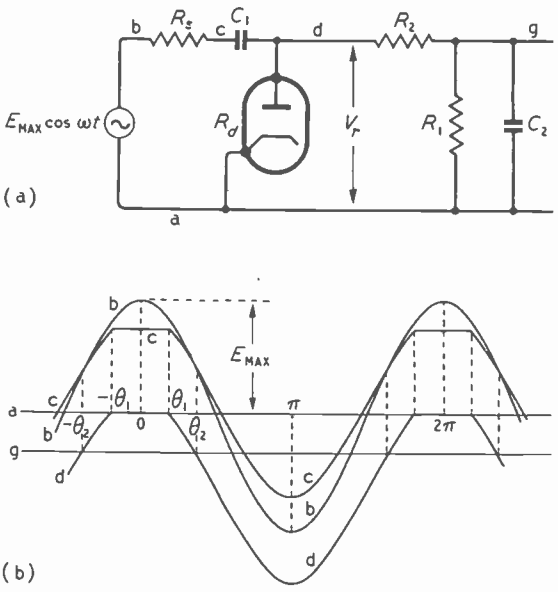

Fig. 12. *Symbols used in discussing Fig.* 4 *circuit, and potential diagram.*

Figs. 1 and 2, fC_1R_1 in Fig. 3, or $fC_1(R_1 + R_2)$ in Fig. 4. Methods of computing η when fCR in Fig. 1 is finite have been shown by Marique[3] and Bell[6], and even although owing to the assumptions made they are only approximate, they are somewhat tedious, especially if R_c is also finite. If R_c is assumed to be zero, the approximation given by Bell is

$$\eta \approx \tfrac{1}{2}\left[1 + \exp.\left(\frac{-(1 - \alpha/2\pi)}{fCR}\right)\right] \approx \tfrac{1}{2}(1 + \cos\alpha)$$

where α is the angle of diode conduction. In Fig. 13 the error, $1 - \eta$, has been plotted against infinite-fCR curve, so that when the R_c error is comparatively large the additional error due to finite fCR is negligible.

Although some initial reduction of η due to finite fCR, as with R_s or R_d, reduces liability to error due to either smaller fCR or greater R_s, as a deliberate policy it is inadmissible because of its being dependent on frequency. The fCR error should be kept within the allowable limit at the lowest frequency of use. A deliberate initial loss caused by augmenting the diode resistance serves not only to reduce resistance error but also the value of capacitance needed to keep the low-frequency error to a stated figure. For example, Fig. 14 shows that if the initial R_c is made equal to $0{\cdot}02R$, the error due to fCR being as low as 5 is only a fraction of 1%, whereas with normal diode and load resistances it would be more than 5%.

Although only the series-diode circuit has been analysed in the references given, the present analysis of the other circuits leads one to suppose that their behaviour would be very similar, at least in the small and moderate error ranges.

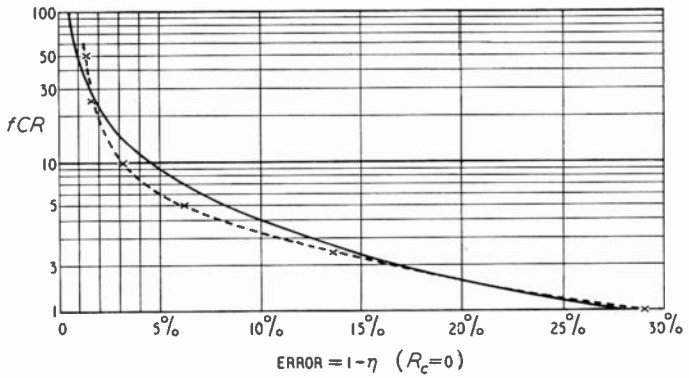

Fig. 13 (above). *The full-line curve is a calculated approximation to the error $(1-\eta)$ caused by fCR in Fig. 5 not being infinitely great, on the assumption that $R_c = 0$. The dotted curve is experimentally obtained, actually with the Fig. 2 circuit and $R_s = 0$ and R_d of the order of 450Ω, but is virtually identical with all four circuits.*

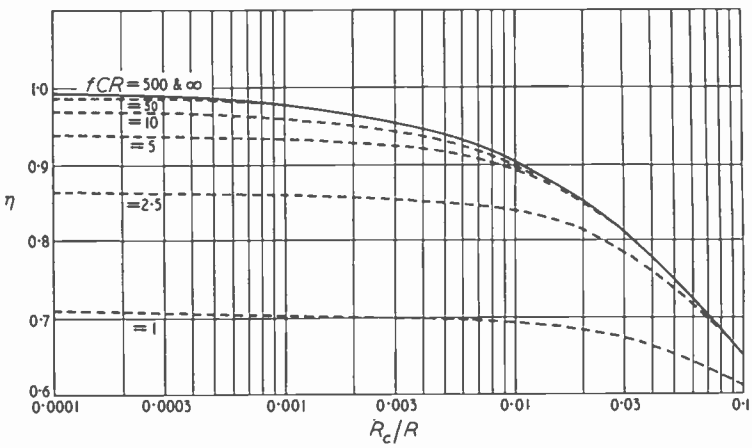

Fig. 14 (right). *Experimental curves of rectifier efficiency as a function of R_c/R at several values of fCR. The curve measured at $fCR = 500$ is virtually identical with the theoretical curve for $fCR = \infty$.*

fCR by this method. To restrict the error to 1% it appears that fCR must be approximately 50; this compares with 1·12 for the ordinary intervalve coupling (Fig. 2 without the diode) for the same loss. It may not always be appreciated that in the diode voltmeter it is necessary for the time constant to be about 50 times as great.

Bell has also shown that the error as calculated above does not increase much with increasing R_c until the error due to R_c with infinite fCR becomes of the same order; from there onwards the finite-fCR curve gradually merges into the

Experimental Procedure

Because it provided a very nearly sinusoidal source of nearly zero impedance, at a low enough frequency to exclude any question of stray capacitance, the 50-c/s public supply was used. An EA50 diode was used, because of its low forward resistance. The z.f. output was measured on the 50-V range of the low-admittance instrument previously described[8].

In plotting the experimental points in Figs. 6 and 11, two small but appreciable differences between the ideal and experimental conditions were allowed for:

(i) The finite forward resistance of the diode. Under the conditions of measurement, 450 Ω was estimated to be a reasonable allowance for diode and source combined, and this figure was added to all values of R_s inserted.

(ii) The finite time constant. The one disadvantage of using a frequency as low as 50 c/s is that any fCR sufficiently near infinity to cause no perceptible error has the effect of making readings excessively sluggish, and therefore most of the readings were taken with $fCR = 50$ and the resulting error approximately calculated and allowed for. This allowance was itself checked experimentally by a few readings with fCR about 10 times greater.

Conclusions

(1) The error, or reduction in rectification efficiency η, due to series source resistance, is the same in the simple shunt circuit (Fig. 2) as in the series circuit (Fig. 1). This theoretical conclusion is satisfactorily supported by experimental readings (Fig. 6).

(2) Exactly the same error is caused in the shunt circuit if the resistance is in series with the diode instead of the source. If the resistance is divided between the two positions there is a difference in error, but unless the total resistance is more than one tenth of the diode load resistance this difference is negligible. This conclusion is confirmed by readings not shown.

(3) If the diode resistance in either circuit is augmented, liability to source-resistance error is reduced (Fig. 8). Experimental results show that a tenfold reduction in error obtained in this way, when the load resistance R is 15 MΩ, reduces the maximum frequency at which stray capacitance is not liable to cause error to a few kc/s. For a threefold reduction the corresponding frequency is about 20 kc/s.

(4) The addition to the simple shunt circuit of the filter R_2C_2 of the form in either Fig. 3 or Fig. 4, affects both source-resistance errors and effective input resistance. The error increases, and input resistance decreases, with the ratio R_1/R_2, if the equivalent of R in Figs. 1 and 2 is regarded as R_1 in Fig. 3 and $R_1 + R_2$ in Fig. 4. The theory for both circuits is satisfactorily supported by experimental readings (Fig. 11). With normal values, the error curve up to a few per cent (Fig. 7) is sufficiently accurate for all four circuits.

(5) In all the foregoing, fCR, fC_1R_1 and fC_2R_2 are assumed infinite. In Figs. 3 and 4, $fC_2R_2 = 2$ is sufficiently near infinity to make negligible difference to the output voltage, but an appreciable error is caused by fCR or fC_1R_1 as high as 50. Experimental measurements of the effect of varying fCR (Figs. 13 and 14) differ appreciably from those calculated by Bell's method[6] (Fig. 13), and also from those by Marique's method[3,7] (both for the series circuit only), presumably because of the simplifying assumptions. The measured effects in the shunt circuit are, within readable limits, the same as in the series circuit. Diode resistance reduces not only source-resistance error as in (3) but also—and in comparable conditions to a greater extent—the low-frequency error due to small fCR or fC_1R_1.

(6) The effects of the filter C_2R_2 on fC_1R_1 error has not been analysed theoretically, but experimental results show that qualitatively they are the same as for R_s error (4) and quantitatively somewhat greater.

REFERENCES

[1] F. M. Colebrook, "The Theory of the Straight Line Rectifier", *Wireless Engineer*, November 1930, pp. 595-603.
[2] J. R. Nelson, "Some Notes of Grid Circuit and Diode Rectification", *Proc. Inst. Radio Engrs*, June 1932, Fig. 3.
[3] J. Marique, "Notes on the Theory of Diode Rectification", *Wireless Engineer*, January 1935, pp. 17-22.
[4] F. C. Williams, "Free Oscillations of a Resonant Circuit Loaded by a Diode Rectifier", *Wireless Engineer*, August 1937, Sec. 2. pp. 403-4.
[5] F. C. Williams, "The Modulation Response and Selectivity Curves of a Resonant Circuit Loaded by a Diode Rectifier", *Wireless Engineer*, April 1938, pp. 189-197.
[6] D. A. Bell, "Diode as Rectifier and Frequency Changer", *Wireless Engineer*, October 1941, pp. 395-404.
[7] K. R. Sturley, "Radio Receiver Design", 1943, Vol. 1, pp. 350-370. Chapman & Hall, London.
[8] M. G. Scroggie, "Valve Voltmeter Without Calibration Drift", *Wireless World*, January 1952, pp. 14-18.
[9] M. G. Scroggie, "Valve Voltmeter—The Rectifier Section", *Wireless World*, March 1952, pp. 89-94.
[10] M. G. Scroggie, "The Diode Rectifier in Valve Voltmeters", *Wireless World*, June and July 1954, pp. 284-286 & 339-343.

SYMPOSIUM ON ELECTROMAGNETIC WAVES

On 20th–25th June, an international symposium on electromagnetic-wave theory is to be held in Ann Arbor at the University of Michigan and is being sponsored by the University and Commission VI of the International Scientific Radio Union. Those who wish to read papers should submit abstracts of not more than 200 words by 31st March to the Chairman, K. M. Siegel, Willow Run Research Center, University of Michigan, Ypsilanti, Michigan, U.S.A.

The main topics will be millimetre-wave properties, propagation in doubly-refracting media in waveguides, boundary-value problems of diffraction and scattering, fundamental aerial theory, forward and multiple scattering. Further details are obtainable from J. W. Crispin, Jun., University of Michigan, Ann Arbor, Michigan, U.S.A.

ABSTRACTS AND REFERENCES INDEX

The Index to the Abstracts and References published throughout 1954 will be supplied with the March issue, but will be detachable so that it can be bound with the 1954 volume. Included with the Index is a selected list of journals scanned for abstracting, with publishers' addresses.

CORRESPONDENCE

Letters to the Editor on technical subjects are always welcome. In publishing such communications the Editors do not necessarily endorse any technical or general statements which they may contain.

Multiloop Feedback Amplifiers

SIR,—Mr. Cutteridge's result, in your November issue, for the stability of multiloop-feedback systems follows at once from a simple consideration of the characteristic equation of the system. For the arrangement of his Fig. 1(c) we have the characteristic equation $1 - A_1\beta_1 - A_2\beta_2 + A_1A_2\beta_1\beta_2 - A_1A_2\beta_3 = 0$ and as $A_1\beta_1$, etc. contain neither poles nor zeros in the right-half plane, then only one diagram is required to determine if there are zeros of $1 - A_1\beta_1 - A_2\beta_2 + A_1A_2\beta_1\beta_2 - A_1A_2\beta_3$ in the R.H. plane.

The normal Nyquist procedure in effect considers the characteristic equation in the form $(1 - A_1\beta_1)(1 - A_2\beta_2)[1 - Y\beta_3] = 0$ where $Y = A_1A_2/(1 - A_1\beta_1)(1 - A_2\beta_2)$ is the transfer function of the forward part of the sequence including the two internal feedback loops. Again, we require for stability that $1 - Y\beta_3$ should have no zeros in the R.H. plane but now $1 - Y\beta_3$ may have poles in the R.H. plane. The application of the full theorem of Cauchy dealing with the excess of the zeros over the poles is then required. The poles of Y in the R.H. plane (namely the zeros of $1 - A_1\beta_1 - A_2\beta_2 + A_1A_2\beta_1\beta_2$ in the R.H. plane) require to be determined previously either by a diagram or by Routh's criterion. Adopting a graphical method, a minimum of two diagrams would be required, therefore, in using the normal Nyquist approach for multiloop systems.

It is worthy of note, however, that using the inverse Nyquist method the characteristic equation becomes $A_1A_2(1/Y - \beta_3) = 0$ and the zeros of $1/Y - \beta_3$ in the R.H. plane may be established by using only one diagram, as the inverse transfer function $1/Y$ has no poles in the R.H. plane. There is thus no distinction in the approach to the stability investigation of single loop or multiloop systems if the inverse transfer function is considered, as, given only minimum-phase elements, $1/Y$ has no poles in the R.H. plane.

A. J. O. CRUICKSHANK.

Department of Electrical Engineering,
Queen's College,
Dundee.
8th December 1954.

The Rotating Magnet

SIR,—Some of the arguments used by Professor Howe in the October Editorial on the rotating magnet appear sufficiently interesting to warrant further discussion.

"Leaving all mathematics aside and looking at the experiment from a common-sense point of view", imagine a wide, thin, long bar magnet rotated about its longitudinal axis. In this case "it seems almost incredible that anyone can seriously maintain" that the field does not rotate with the magnet. Now if the magnet be ground down, while rotating, to a circular bar magnet, we can scarcely suppose the rotation to cease when symmetry is achieved.

However, since it makes no difference to the calculated value of the e.m.f. whether it be regarded as induced in the external circuit by the rotating field, or in the "primitive generator" by the stationary field, it is not clear why the materialistic engineer should not seriously maintain either viewpoint. In particular, the substitution of a stationary solenoid by Professor Howe for the rotating magnet appears to beg the question of the rotation or non-rotation of the field, and can, therefore, scarcely be expected to throw light on the matter.

A detailed analysis of both systems of thought is given by Professor Cullwick ("The Fundamentals of Electro-Magnetism", Cambridge University Press, 1939, pp. 116–119 and Appendix III, pp. 321–341), together with an experimental result (H. A. Wilson and M. Wilson, *Roy. Soc. Proc. A.*, 1913, Vol. 39, pp. 99–106), which is claimed to support the rotating field theory against the fixed field theory.

Professor Howe regards it as "fantastic to expect the electrons in the external circuit to discriminate between the fields produced by the solenoid and the permanent magnet". However true this may be in this particular case, it would be unfortunate if it gave the impression of general truth for long current paths or for complete circuits. If, for example, the line integral of the field be taken along the external conductor and over the surface of the magnet or circular copper rod (in the proposed modified experiment), a major difference is at once apparent. For the first case the integral is zero, while in the second case it is proportional to the ampere-turns of the solenoid. This difference becomes of importance in comparing solenoidal and permanent-magnet focusing lenses for electron beams, where the angular tilt of the electron beam produced by tilting the lens is finite for electro-magnets but zero for permanent magnets. The result is a difficulty in beam centring when permanent magnets are used, and is a clear example of electrons distinguishing between the two types of field. Mr. P. Hammond, in his reply to the I.E.E. discussion (*Proc. Instn elect. Engrs*, Part I, No. 130, July 1954, p. 165) of his excellent paper also picks on this point in "It must be stressed that a bar magnet is not identical with a solenoid".

H. B. S. BRABHAM.

Research Laboratories,
The General Electric Co. Ltd.,
Wembley.
13th December 1954.

[If Mr. Brabham will delve into the *Wireless Engineer* archives and look at the Editorial of August 1933 he will find the following. "If the source of heat, or light, or magnetism, is not uniform about the axis of rotation [for example, with a rectangular magnet] the result of the rotation might be regarded by a superficial observer as an obvious proof of the rotation of the illumination, or temperature, or magnetic induction, but a closer consideration will show that these conditions are merely undergoing such changes at every point that their inequalities of distribution rotate. The illumination, or temperature, or magnetic induction at A may now be equal to what it was a moment ago at B, but it does not follow that the illumination, or temperature, or magnetic induction which now exists at A is actually that which was at B, and that it must necessarily have rotated; in fact, such a statement appears meaningless. We can see then no escape from the conclusion that the question whether the magnetic field rotates with the magnet or not can have no answer because it has no meaning". Also, on the previous page, "There appears to be no justification for picturing the space as filled with concrete lines of magnetic induction fixed like bristles in some mysterious way to the magnet and forced to rotate with it". Then near the foot of col. 1, p. 410, "The phenomena can thus be explained by the movement of electrons in magnetised space without doing violence to one's powers of imagination by endowing with revolution a condition of space which undergoes no change", and at the foot of col. 2,

"It would doubtless be possible to explain all these phenomena without the conception of a magnetic field, as they are all primarily due to the relative motion of electrons".

In a letter to *The Electrician* of 9th Sept. 1938, Professor Cullwick said "Are not electric and magnetic fields merely hypotheses . . . illogically endowed with reality?" to which we replied (16th Sept.) "How experiments made to determine the rotation or non-rotation of a hypothesis illogically endowed with reality can be anything but chimera-chasing passes my comprehension".

Mr. Brabham's references to Professor Cullwick's book are rather out of date and may mystify some readers, as the 1939 edition was replaced in 1949 by a second edition from which the Appendix III of 20 pages to which he refers was deleted. With regard to his remark that our substitution of a stationary solenoid for the rotating magnet appears to beg the question, we agree that it is an over-simplification, but it was introduced for comparison with the more complex rotating magnet.

There is a slight misunderstanding in Mr. Brabham's criticism of our statement that it is fantastic to expect the electrons in the external circuit to discriminate between the fields produced by the solenoid and the permanent magnet. This statement was intended to refer to the electric field and not to the magnetic field. Obviously the line integral of H around a closed path linking any turns of the coil will depend on the current linked. Inside the rotating armature the electrons are interested in the magnetic field in which they are rotating, but the forces on the almost stationary electrons in the stationary external circuit depend on the electric fields in which they are situated, and these are the fields to which we were referring. It would have made it clearer if we had inserted the word 'electric'.

If we apply the relativistic point of view to the occurrences within the rotating magnet, we have an electric field due to the apparent displacement of the magnetizing electrons due to their rotation; this electric field exactly counterbalances the electromagnetic force on the rotating free electrons, and thus cancels the ordinary source of induced e.m.f. This relativistic electric field can be pictured, however, as taking over the duties of the free electrons, so far as they were responsible, by their distribution, for maintaining the potential difference between the positive and negative terminal portions of the magnet surface. When current flows in the external circuit electrons pass through the magnet as they did in the non-relativistic picture.

In view of the long letter in our January issue in which Professor Cullwick discussed the application of relativity principles to the problem and to which we referred in the January Editorial, we do not propose to discuss the matter further here. G. W. O. H.]

MEETINGS

I.E.E.

7th February. "The Problem of Radio Interference", discussion to be opened by C. W. Sowton, B.Sc.

9th February. "A Study of Commercial Time Lost on Transatlantic Radio Circuits due to Disturbed Ionospheric Conditions", by J. K. S. Jowett, B.Sc.(Eng.) and G. O. Evans, B.Sc. "Performance Characteristics of High-Frequency Radio Telegraph Circuits", by A. M. Humby, C. M. Minnis, M.Sc. and R. J. Hitchcock, B.A.

14th February. "Teaching Faraday's Law of Electromagnetic Induction", discussion to be opened by P. Hammond, M.A, at 6 o'clock.

21st February. "Recent Search for and Salvage of the Comet Aircraft near Elba", informal lecture by Commander C. G. Forsberg, R.N. and G. G. MacNeice, B.Sc.

2nd March. "Some Comparative Directional Measurements on Short Radio Waves over Different Transmission Paths" and "Some Aspects of the Rapid Directional Fluctuations of Short Radio Waves Reflected at the Ionosphere", by E. N. Bramley, M.Sc. "On the Rapidity of Fluctuations in Continuous Wave Radio Bearings at High Frequencies", by W. C. Bain, M.A., B.Sc., Ph.D. "Sources of Error in U-Adcock High-Frequency Direction Finding", by K. C. Bowen, M.A.

These meetings will be held at the Institution of Electrical Engineers, Savoy Place, Victoria Embankment, London, S.W.1, and will commence at 5.30 except where otherwise stated.

Brit.I.R.E.

23rd February. "A Versatile Electronic Engine Indicator", by R. K. Vinycomb, B.Sc. Meeting will be held at 6.30 at the London School of Hygiene and Tropical Medicine, Keppel Street, Gower Street, London, W.C.1.

STANDARD-FREQUENCY TRANSMISSIONS

(Communication from the National Physical Laboratory)

Values for December 1954

Date 1954 December	Frequency deviation from nominal: parts in 10^8		Lead of MSF impulses on GBR 1000 G.M.T. time signal in milliseconds
	MSF 60 kc/s 1429-1530 G.M.T.	Droitwich 200 kc/s 1030 G.M.T.	
1	−0·7	+4	+ 9·3
2	NM	+3	+ 9·0
3	−0·9	+3	+ 9·4
4	−0·9	+4	NM
5	−0·9	+4	NM
6	−0·8	+5	+ 9·1
7	−1·3	+6	+ 7·9
8	−1·2	+1	+ 7·2
9	−1·2	0	+ 6·5
10	−1·1	−1	+ 5·4
11	NM	−1	NM
12	NM	0	NM
13	−1·1	0	+ 3·5
14	−1·2	−1	+ 2·8
15	−1·1	−1	+ 1·0
16	−1·2	−2	− 0·6
17	−1·2	−2	− 2·6
18	NM	−2	NM
19	NM	−2	NM
20	−1·0	−1	− 6·5
21	−1·0	−1	− 8·0
22	−1·0	0	− 9·0
23	−1·0	−1	−10·7
24	−1·0	0	NM
25	−1·0	−2	NM
26	−1·0	−3	NM
27	−1·0	−4	NM
28	−1·0	−3	NM
29	−1·1	−4	−16·1
30	−1·1	−5	−17·5
31	−1·0	−5	−18·9

The values are based on astronomical data available on 1st January 1955.

NM = Not Measured.